Quaternary Science Reviews 137 (2016) 234–254

Contents lists available at ScienceDirect

Quaternary Science Reviews

journal homepage: www.elsevier.com/locate/quascirev

Synchronisation of sedimentary records using tephra: A postglacial tephrochronological model for the Chilean Lake District

Karen Fontijn [a, b, *], Harriet Rawson [a], Maarten Van Daele [b], Jasper Moernaut [c, d], Ana M. Abarzúa [c], Katrien Heirman [e], Sébastien Bertrand [b], David M. Pyle [a], Tamsin A. Mather [a], Marc De Batist [b], Jose-Antonio Naranjo [f], Hugo Moreno [g]

[a] Department of Earth Sciences, University of Oxford, UK
[b] Department of Geology, Ghent University, Belgium
[c] Instituto de Ciencias de la Tierra, Facultad de Ciencias, Universidad Austral de Chile, Valdivia, Chile
[d] Geological Institute, ETH Zürich, Switzerland
[e] Geological Survey of Denmark and Greenland, Department of Geophysics, Øster Voldgade 10, DK-1350 Copenhagen K, Denmark
[f] SERNAGEOMIN, Santiago, Chile
[g] OVDAS – SERNAGEOMIN, Temuco, Chile

ARTICLE INFO

Article history:
Received 30 July 2015
Received in revised form
1 February 2016
Accepted 15 February 2016
Available online 27 February 2016

Keywords:
Southern Volcanic Zone
Lake District
Patagonia
Tephrochronology
Eruptive history
Postglacial

ABSTRACT

Well-characterised tephra horizons deposited in various sedimentary environments provide a means of synchronising sedimentary archives. The use of tephra as a chronological tool is however still widely underutilised in southern Chile and Argentina. In this study we develop a postglacial tephrochronological model for the Chilean Lake District (ca. 38 to 42°S) by integrating terrestrial and lacustrine records. Tephra deposits preserved in lake sediments record discrete events even if they do not correspond to primary fallout. By combining terrestrial with lacustrine records we obtain the most complete tephrostratigraphic record for the area to date. We present glass geochemical and chronological data for key marker horizons that may be used to synchronise sedimentary archives used for palaeoenvironmental, palaeoclimatological and palaeoseismological purposes. Most volcanoes in the studied segment of the Southern Volcanic Zone, between Llaima and Calbuco, have produced at least one regional marker deposit resulting from a large explosive eruption (magnitude ≥ 4), some of which now have a significantly improved age estimate (e.g., the 10.5 ka Llaima Pumice eruption from Llaima volcano). Others, including several units from Puyehue-Cordón Caulle, are newly described here. We also find tephra related to the Cha1 eruption from Chaitén volcano in lake sediments up to 400 km north from source. Several clear marker horizons are now identified that should help refine age model reconstructions for various sedimentary archives. Our chronological model suggests three distinct phases of eruptive activity impacting the area, with an early-to-mid-Holocene period of relative quiescence. Extending our tephrochronological framework further south into Patagonia will allow a more detailed evaluation of the controls on the occurrence and magnitude of explosive eruptions throughout the postglacial.

1. Introduction

Widespread tephra horizons, typically representing ash fallout from large volcanic eruptions, have the potential to form excellent isochronous marker horizons across diverse depositional environments. Tephra deposits which are well characterised in terms of chemical composition and age can be used to synchronise sedimentary archives studied for a variety of applications, including volcanology, palaeoclimatology and palaeoseismology. In volcanology, well-constrained sequences of tephra deposits from one or multiple volcanic centres provide a view of their eruptive behaviour through time, in terms of eruption frequency, style, magnitude, rate, composition, etc. (e.g., Fontijn et al., 2015; Rawson et al., 2015; Schindlbeck et al., 2014), and provide insights into the processes that control the temporal evolution of volcanic activity (e.g., Rawson et al., 2016, and references therein). Highly precise age models are also required for palaeoclimatological, palaeoenvironmental and

* Corresponding author. Department of Earth Sciences, University of Oxford, UK.
E-mail address: Karen.Fontijn@earth.ox.ac.uk (K. Fontijn).

http://dx.doi.org/10.1016/j.quascirev.2016.02.015

palaeoseismological reconstructions based on sedimentary archives. Due to the input of reworked organic material from the watershed into the lakes, or possible CO_2 disequilibrium between lake waters and the atmosphere, radiocarbon dating of sediments is often problematic, and may offset estimated ages from real ages by several 100s to more than 1000 years (e.g., Bertrand et al., 2012; Howarth et al., 2013). In addition to radiocarbon dating of bulk sedimentary organic matter or macrofossil remains, tephra deposits incorporated within lacustrine sediments may be used as a chronological tool. If the chemical composition and relative stratigraphic position of a tephra deposit incorporated in lake sediments can be matched with proximal terrestrial records, the known age of the deposit can be transferred between sections and used to construct precise sedimentary age models and synchronise records with various applications (e.g., Blockley et al., 2012; Davies et al., 2012; Moernaut et al., 2014; Ponomareva et al., 2015; Van Daele et al., 2014, 2015). Precise chronological reconstructions of records containing tephra deposits are also essential to investigate possible feedbacks between volcanism and climate or the local environment (e.g., Henríquez et al., 2015; Huybers and Langmuir, 2009; Jara and Moreno, 2014; Maclennan et al., 2002; Watt et al., 2013a), and causal links between volcanism and tectonic earthquakes (e.g., Eggert and Walter, 2009; Lemarchand and Grasso, 2007; Watt et al., 2009).

Here we present a postglacial tephrochronological model for South-Central Chile, based on integrated records of terrestrial and lacustrine sequences of tephra deposits. The volcanoes in the Chilean Lake District, ca. 38 to 42°S (Fig 1), form part of the Southern Volcanic Zone of the Andes. This area includes some of the historically most frequently active volcanoes in South America, e.g., Villarrica (Van Daele et al., 2014) and Llaima (Schindlbeck et al., 2014), as well as some of the most explosive volcanoes in Southern Chile, e.g., Mocho-Choshuenco (Rawson et al., 2015) and Puyehue-Cordón Caulle (Singer et al., 2008), both of which have had multiple Plinian eruptions in their postglacial history. A critical review of the previously known eruptive records of the southern Chilean and Argentinian volcanoes was presented by Fontijn et al. (2014). Recent studies of Llaima (Schindlbeck et al., 2014) and Mocho-Choshuenco (Rawson et al., 2016) have clearly demonstrated the value of modern detailed postglacial stratigraphic reconstructions of explosive activity at individual volcanic centres or complexes, to understand the temporal controls on eruptive behaviour.

The Chilean Lake District is of primary importance for palaeoseismological reconstructions assessing the recurrence rates of large earthquakes along the Valdivia segment of the Chilean subduction zone (e.g., Moernaut et al., 2007; 2014; Van Daele et al., 2015). Palaeoseismological studies using lacustrine turbidite deposits encountered in sediment archives that also include tephra deposits benefit from tephrochronological synchronisations to obtain the most precise age models and correlations between sections (Moernaut et al., 2014; Van Daele et al., 2015). This benefit also applies to palaeoenvironmental reconstructions. The Chilean and Argentinian Lake Districts have been the focus of numerous palaeoclimatological and palaeoecological (e.g., Bertrand et al., 2008a; Boës and Fagel, 2008; Fletcher and Moreno, 2012; Heusser et al., 1988; 1999; Hoganson and Ashworth, 1992; Iglesias et al., 2012; Moreno, 1997; Moreno et al., 2001; Sterken et al., 2008) studies, all of which have encountered volcanic ash deposits in the sedimentary archives studied. With only a few exceptions (Moreno et al., 2015a), these tephra deposits have however typically not been chemically characterised and so their potential as a tephrochronological tool has remained largely underutilised (Fontijn et al., 2014).

We present new chemical and chronological data for many widespread deposits from large explosive eruptions (typically, eruptions of magnitude 4–6), some of them newly described, including for Quetrupillan and Puyehue-Cordón Caulle volcanoes. Our dataset includes 25 tephra marker horizons that were correlated between sedimentary archives, as well as chemical data for additional smaller-scale units, e.g., from Lanín and Calbuco volcano, that were identified in a limited number of sections. These data may be used as a reference for melt chemical composition at the volcanoes in our study area. Our dataset integrates terrestrial sections with lacustrine archives from multiple lakes, and captures the entire postglacial history of explosive activity impacting the study area, allowing firm correlations to source volcanoes and constraints on eruptive style. Our tephrochronological framework allows a first-order evaluation of the regional-scale eruptive behaviour throughout the postglacial, although relatively small-scale eruptive activity may well be underrepresented in this record. With new and/or improved age estimates of several widespread marker horizons, our age model can also be used to synchronise, fine-tune or recalibrate various chronological reconstructions for non-volcanological purposes across the region.

2. Methods

Systematic stratigraphic logging and sampling of pyroclastic deposits in the field was carried out between 2012 and 2015 in 332 localities covering the area between 38.5°S (N of Llaima volcano) and 41.4°S (in the proximity of Calbuco volcano, Fig 1; Supplementary Table S1). About 75% of the studied localities are in the northern half of this area, roughly at the latitudes of Lago Villarrica, Lago Calafquen and Lago Riñihue, and we mainly focused on pumiceous and/or thick units with presumed wide spatial distribution. From west to east, the logged sections are restricted to an area spanning roughly 100 km across the volcanic range. Due to prevailing westerly winds, most tephra is transported eastward of the volcanoes, and deposited in proximal mountainous localities, and on the Patagonian steppe. In this latter environment, preservation of loose tephra fall deposits is hindered by strong wind erosion (Fontijn et al., 2014). Most sections thus cover the proximal to medial sectors of pyroclastic fall and density current deposits. Characteristics of key units are presented in Table 1; their dispersal is visualised in Supplementary Information S2.

In addition to terrestrial outcrops, visible tephra layers (generally medium to coarse ash, with particle grain size < 2 mm) were sampled from sediment cores obtained by UWITEC piston coring (from an anchored platform) in four different lakes within the Lake District: Laguna Las Ranas, Lago Villarrica, Lago Calafquen and Lago Riñihue (Fig. 1). Gravity (short) cores from the latter three and seven additional lakes (Pullinque, Panguipulli, Ranco, Maihue, Puyehue, Rupanco, Llanquihue) were also sampled. An overview of sampled sediment cores, including previous references, is given in Table 2. Lithologies for some of the sampled sediment cores are presented by Moernaut et al. (2014, 2016), Van Daele et al. (2014, 2015) and Wiemer et al. (2015).

The high frequency eruptive behaviour of regional volcanoes, particularly Villarrica, with relatively small individual events, results in an abundance of tephra deposits of restricted spatial distribution, and therefore limited tephrochronological potential, in particular in the lake sediment cores of Lago Villarrica (Fig. 1). Sampling of the Lago Villarrica cores was therefore limited to the thickest (>0.5 cm) and/or grey-coloured tephras, the latter presumed to be representing distal deposits of widespread silicic units from volcanoes other than Villarrica, which produces dominantly basaltic andesitic tephras. In sediment cores from other lakes, all visible tephras were sampled.

Major element compositions of glasses from tephra samples from both terrestrial and lacustrine sections were determined by

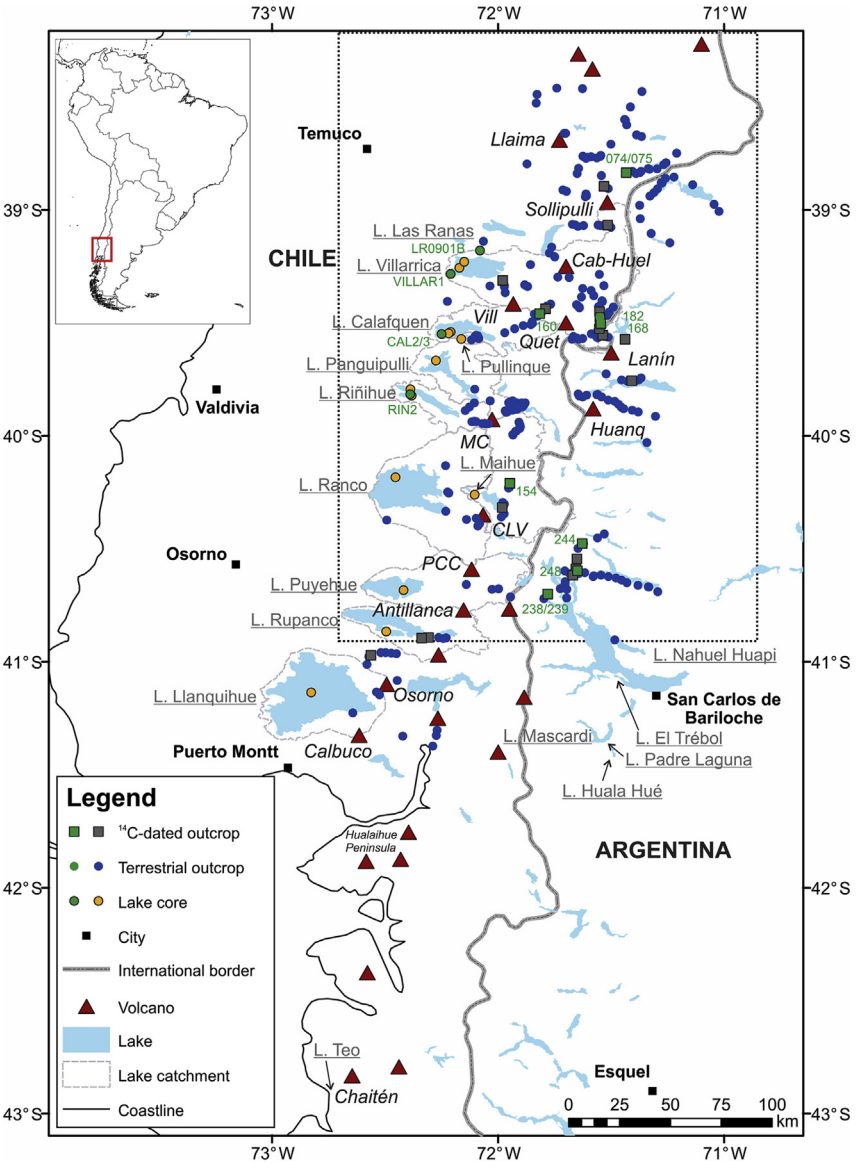

Fig. 1. Geographic setting of the Chilean Lake District showing sampled terrestrial outcrops (blue dots), including those sub-sampled for ^{14}C dating (grey squares), and sampled lake sediment core localities (yellow dots). Similar symbols in green indicate sections represented in Fig. 3. "CLD" (indicating terrestrial sections in Fig. 3) has been omitted from terrestrial section names for brevity. Volcanoes (black, italics) and lakes (grey, underlined) of importance to this study are named. Cab-Huel: Caburgua Huelemolle; Vill: Villarrica; Quet: Quetrupillan; Huanq: Huanquihue Group; MC: Mocho-Choshuenco; CLV: Carrán-Los Venados; PCC: Puyehue-Cordón Caulle. Dashed grey lines indicate lake catchments for the main Chilean lakes in the region. Dotted frame highlights area represented in Fig. 4. (For interpretation of the references to colour in this figure legend, the reader is referred to the web version of this article.)

Electron Microprobe (EMP) using a JEOL JXA-8600 Superprobe at the Research Laboratory for Archaeology and the History of Art, or a JEOL JXA-8800R at the Begbroke Science Park, both at the University of Oxford, UK. Samples were gently crushed, wet-sieved at 20 μm (lacustrine tephras) or 80 μm (terrestrial tephras), dried at 60 °C and cold-mounted in pre-drilled EpoFix resin discs using the procedures outlined by Lowe (2011). Quantitative chemical analyses on polished discs were only obtained after visual inspection of textures using backscatter electron imaging on a secondary electron microscope (JEOL JSM-840A, Department of Earth Sciences, University of Oxford, UK). Samples in which the groundmass was too crystalline were not analysed. These omitted samples were mainly basalts and basaltic andesites sourced from Llaima, Villarrica, Quetrupillan, Carrán-Los Venados and Osorno. EMP analyses were performed on carbon-coated polished discs using a defocused beam centred on glassy patches. Care was taken to avoid microlite-bearing or devitrified parts of the samples. Analyses were run at 15 kV accelerating voltage, 6 (or 4) nA beam current, and with a 10 (or 5) μm beam size. All elements were counted on-peak for 30 s, except for Na (12 s, and analysed first to minimise alkali loss), P (60 s), Mn and Cl (50 s). Off-peak background count times were half the peak counting times. Data quality was continuously monitored by secondary glass standards analysed at the start, regularly during and at the end of each analytical session. Average measured values on secondary standards generally fall within 2 standard deviations of published preferred values (Jochum et al., 2006). Error bars on the measurements of unknowns were calculated using the relative standard deviation of the measured values on the standard which is closest in composition to the sample. 25 to 30 individual points were attempted per sample. Every analysis was carefully screened to evaluate the potential influence of hidden crystals (mostly plagioclase, olivine or clinopyroxene) or voids. Only analyses with

Table 1
Main characteristics of widespread tephra units that allow synchronisation of terrestrial and lacustrine records in the Chilean Lake District. Most units are dispersed at least 30 km away from source and preserved in both terrestrial and lacustrine environments (Supplementary Information S2). Identification of units in multiple localities is constrained by glass major element composition in combination with relative stratigraphic position. Modelled age range, at the 95.4% confidence interval, results from Bayesian modelling of radiocarbon dates and a set of known calibrated ages (e.g., from varve stratigraphy, Van Daele et al., 2014) in relation to the stratigraphy of the tephra deposits. Modelling was performed in OxCal 4.2 (Bronk Ramsey, 2009) using the SHCal13 calibration curve of Hogg et al. (2013).

Source volcano	Unit	Description (terrestrial)	Description (lacustrine)	Glass composition	Volume (km^3)	VEI	Magnitude	Dispersal axis	Max observed distance from source (km)	Modelled age (cal BP; 95%)	Modelled age μ (cal BP)	Modelled age 1σ (cal BP)	Previous age estimates (cal ka BP, ± 1σ)	Remarks	Key reference
Llaima	Llaima Pumice	lithic-poor pumice lapilli breccia (fall deposit), slightly reversely graded at the base – bottom 70–80% white to cream-coloured highly vesicular and very crystal-poor pumice; transition zone with banded and grey pumice clasts; top 20–30% dominated by brown-black dense scoria lapilli; medium-coarse black and cream-coloured ash at the very base of the deposit; in proximal localities the fall deposit is overlain by poorly sorted matrix-supported deposits showing low-angle cross- and dune bedding (pyroclastic density current deposits)	medium black ash	bimodal: pumice dacite (~69–70% SiO_2), scoria andesite (~59–60% SiO_2)	4.7	5	5.6	SSE	70 (downwind); 70 (crosswind)	10,338–10,586	10,450	67	8.20 ± 0.17; 9.85 ± 0.16; 10.12 ± 0.10		Naranjo and Moreno 1991, Naranjo and Moreno 2005
Sollipulli	Alpehue Pumice	coarse poorly sorted white pumice lapilli breccia (fall deposit); proximal sections dominated by very poorly sorted matrix-supported crudely bedded deposits with lots of charcoal (ignimbrite facies); white crystal-rich pumice with large feldspar crystals; ~10% lithics, some hydrothermally altered clasts	coarse white pumiceous ash	rhyolite (~73.5–74.5% SiO_2)	7.5 (PDC)* + 3.6 (fall)	6	6.2	ENE	45 (downwind); 65 (crosswind)	2843–3056	2951	53	2.93 ± 0.09; 2.94 ± 0.09; 2.98 ± 0.08; 2.99 ± 0.09		Naranjo et al., 1993
Caburgua-Huelemolle	CabHuel	parallel bedded coarse ash – scoria lapilli deposits, bedding on cm-dm scale; individual units not tightly linked to specific centres	2 subsequent units of medium – coarse black ash	basaltic andesite (~53% SiO_2)		*3–4*	*3–4*		40	10,312–10,480	10,381	44	*6.8 –9.5*	modelled as single eruption – likely representing multiple eruptions, possibly from different centres, relatively closely spaced in time	
Villarrica	Chaimilla	series of multiple coarse scoria lapilli breccia deposits (fall deposits) interbedded with finer ash-rich and fine lapilli horizons		basaltic andesite (~55–56% SiO_2)	0.6*	4	4.8	NW	30 (downwind)	3091–3446	3292	93	<3.35 ± 0.06	glass composition difficult to fingerprint due to abundance of microphenocrysts; presence in lake sediment cores not confirmed by chemical composition but inferred from stratigraphic position	Costantini et al., 2011

(*continued on next page*)

Table 1 (*continued*)

Source volcano	Unit	Description (terrestrial)	Description (lacustrine)	Glass composition	Volume (km^3)	VEI	Magnitude	Dispersal axis	Max observed distance from source (km)	Modelled age (cal BP; 95%)	Modelled age μ (cal BP)	Modelled age 1σ (cal BP)	Previous age estimates (cal ka BP, ± 1σ)	Remarks	Key reference
	Pucón Ignimbrite	*Ignimbrite Facies*: dark grey, massive, generally matrix-supported deposits with (breadcrusted) scoriaceous bombs, often containing granitoid xenoliths; *Fall facies*: tripartite horizon, bottom coarse scoria lapilli fall, middle indurated ash-rich unit with accretionary lapilli, top scoria lapilli fall	medium – coarse black ash	basaltic andesite (~57% SiO_2)	3.1 (PDC)* + 0.2 (fall)*	5	5.7	NNE (fall), radial (PDCs)	40 (tripartite fall)	3927–4044	3996	27	3.74 ± 0.08; 3.82 ± 0.10; 3.92 ± 0.06; 3.95 ± 0.09; 4.00 ± 0.08; 4.04 ± 0.11; 4.09 ± 0.13	tripartite fall unit not described by Silva Parejas et al. (2010) – not clear where it sits stratigraphically with respect to the ignimbrite facies, and whether it corresponds to the basal scoria fall unit – fits better with descriptions of Chaimilla deposits (Costantini et al., 2011) but chemically different; could Pucón Ignimbrite and Chaimilla belong to the same sequence of events?	Silva Parejas et al., 2010; Moreno and Clavero 2006
	Licán Ignimbrite	reddish brown, massive to crudely bedded matrix-to-clast-supported units with (breadcrusted) crystal-poor scoria bombs; abundant granitoid xenoliths		andesite (~58 –60% SiO_2)	10 (PDC)*	6	6.2	radial	35	16,549–16,877	16,710	84	16.56 ± 0.17; 16.62 ± 0.18; 16.63 ± 0.13; 16.67 ± 0.17; 16.69 ± 0.18; 16.70 ± 0.17; 16.79 ± 0.14; 16.88 ± 0.17; 16.91 ± 0.18	glass composition difficult to fingerprint due to abundance of microphenocrysts	Lohmar et al., 2007, Lohmar et al. 2012; Moreno and Clavero 2006
Quetrupillan	Quet5	cream-coloured pumice lapilli breccia (fall deposit), lithic-rich, with obsidian lithics		dacite (~66 –67% SiO_2)			*3*	ENE	15	1587–1790	1695	48		locally preserved unit	
	Puesco Pumice	cream-coloured pumice lapilli breccia (fall deposit), generally lithic-poor, but in some localities lithic-rich in small grain size fractions (<5 mm), mainly obsidian lithics, crystal-poor pumice, in many outcrops reworked at top; covered with fine cross-bedded ash-rich deposits (PDC "surge" deposits)		dacite (~67 –68% SiO_2)	0.3	4	4.4	E	20 (downwind); 35 (Lago Calafquen, possibly washed in)	1850–1987	1915	35	1.50 ± 0.08	locally preserved unit, likely corresponds to Quetrupillan unit described by Pavez (1997)	Pavez 1997
	Quet3	white to cream-coloured small pumice lapilli concentration		rhyodacite (~69–70% SiO_2)		*3*	*3*		15 (if from Quetrupillan); 60 (if Sollipulli)	12,567–12,708	12,608	29		locally preserved unit	
	Quet2	white pumice concentration in ash matrix (PDC deposit), relatively crystal-rich pumice		rhyolite (~69 –70% SiO_2)		*3*	*3*		15 (if from Quetrupillan); 60 (if Sollipulli)	12,582–15,597	13,295	932		locally preserved unit	
	Quet1	black medium ash covering grey ash with small pumice lapilli		rhyolite (~71 –72% SiO_2)		*3*	*3*		15 (if from Quetrupillan); 60 (if Sollipulli)	16,189–16,748	16,492	154		locally preserved unit	

Huanquihue Group	Achen Nihue	coarse ash to small scoria lapilli deposit (fall deposit), associated with scoriaceous a'a lava flow	medium black ash	basaltic trachyandesite (~55% SiO_2)		*3*	*3*		80	349–370	359	5	0.19 ± 0.12; 359 varve BP	widespread marker horizon in lacustrine sediments	
	HUA1	*(no terrestrial exposures known)*	medium black ash	basaltic trachyandesite (~55% SiO_2)		*3*	*3*		65	4028–4212	4117	44		marker horizon in lacustrine sediments, not found on land	
Mocho-Choshuenco	MC23 (Arauco Pumice)	well sorted scoria lapilli breccia (fall deposit)	medium-coarse grey ash	andesite (~59% SiO_2)		3	3	N	50 (Lago Calafquen)	379–401	390	5	0.22–0.46		Rawson et al., 2015
	MC18 (HuaHum Pumice)	lithic-poor pumice lapilli breccia (fall deposit), in proximal localities overlain by poorly sorted, matrix-to-clast-supported pumice and ash deposits (PDC deposits)		andesite-dacite (~62% SiO_2)	0.4*	4	4.6*	NE, SE	30	1005–1325	1168	86	1.16–1.38		Rawson et al., 2015
	MC15 (Enco Pumice)	lithic-poor black-grey scoria lapilli breccia (fall deposit), interbedded with laminated coarse ash – small lapilli horizons, overlain by poorly sorted matrix-supported deposits with some cross-bedding in places, occasional accretionary lapilli	medium black ash	andesite (~60–61% SiO_2)	0.7 (fall)* + 1.0 (PDC)*	5	5.0*	SE (fall), radial (PDC)	30	1475–1694	1587	58	1.47–1.70		Rawson et al., 2015
	MC4 (Neltume Pumice)	lithic-poor pumice lapilli breccia (fall deposit)	coarse white ash, black crystals concentrated at top	rhyodacite (~69–71% SiO_2)	5.3*	5	5.7*	NNE	80 (downwind)	10,568–11,960	11,398	404	10.39–12.39		Rawson et al., 2015
Puyehue-Cordón Caulle	Mil Hojas	lithic-rich (obsidian) white pumice lapilli breccia with strong grain size variations: parallel bedded alternations of pumice lapilli and coarse ash (fall deposits); bottom unit most prominent pumice fall	medium-coarse black ash	rhyodacite (~69–71% SiO_2)	1.3	5	5.0	N?	145 (Lago Villarrica)	672–1015	840	88	1.03 ± 0.05		Singer et al., 2008
	PCC4	*(no terrestrial exposures known)*	medium black ash	dacite (~67–68% SiO_2)		*4*	*4*		115 (Lago Calafquen)	2955–3264	3087	80			
	Ranco Pumice	relatively lithic-rich (~20%, obsidian chips and microcrystalline lava chunks) pumice lapilli breccia (fall deposit), crystal-poor cream-coloured pumice	coarse beige ash	rhyolite (~70–71% SiO_2)	1.0 (N lobe) + 2.6 (E lobe)	5	5.5	N, E	145 (Lago Villarrica)	4099–4677	4353	163			
	PCC2	reversely graded, lithic-poor (mostly lava chunks, few obsidian pieces) pumice lapilli breccia, crystal-poor cream-coloured pumice	poorly sorted, indurated matrix-supported with dispersed pumice lapilli (lahar/reworked)	rhyolite (~71–72% SiO_2)	1.0*	5	4.9	E, N?	125	6266–6590	6419	82	6.4 ± 0.9; 6.9 ± 1.6; >6.20 ± 0.09; <6.66 ± 0.09; <7.12 ± 0.08	likely corresponds to Pr2 of Singer et al. (2008)	Singer et al., 2008
	PCC1	pumice lapilli breccia, generally lithic-poor, in some places lithic-rich in upper half, some grain size variations, crystal-poor yellow-orange altered pumice		rhyodacite (~70% SiO_2)	0.5*	4	4.6	E?	50	10,295–10,455	10,356	41	10.44 ± 0.08	only medial-proximal exposures, likely corresponds to Pr1 of Singer et al. (2008)	Singer et al., 2008

(*continued on next page*)

Table 1 (*continued*)

Source volcano	Unit	Description (terrestrial)	Description (lacustrine)	Glass composition	Volume (km^3)	VEI	Magnitude	Dispersal axis	Max observed distance from source (km)	Modelled age (cal BP; 95%)	Modelled age μ (cal BP)	Modelled age 1σ (cal BP)	Previous age estimates (cal ka BP, ± 1σ)	Remarks	Key reference
Antillanca Group	Ant2	zoned clast-supported unit (fall deposit) with light brown pumice component at the bottom, middle part crudely bedded coarse ash – small scoria lapilli, top part coarser dense scoria lapilli; three parts appear to be separated by soil horizons in some places (interpreted as breaks in the eruption)		andesite-dacite (~63–64% SiO_2)	0.1 (3.0)*	5	5.5	E?	50	1766–1915	1849	37	>1.62 ± 0.05; <1.89 ± 0.05	likely corresponds to An-A of Watt et al. (2013a); middle, lithic-rich part of this unit was previously (Singer et al., 2008) thought to originate from the Rayhuen crater.	Lara et al., 2006; Singer et al., 2008
	PBN (Playas Blancas Negras)	zoned pumice lapilli breccia, slightly reversely graded at the base, normal grading towards the top (fall deposit) - dominantly bright white amphibole-phyric pumice, top 20% dark brown scoria lapilli		pumice: rhyolite (~71–72% SiO_2)	5.2	5	5.6	ENE	70	2203–2283	2244	20	2.16 ± 0.09; 2.17 ± 0.11; >2.17 ± 0.09; >2.20 ± 0.08; >2.22 ± 0.06; >2.22 ± 0.10; <2.42 ± 0.09; <2.84 ± 0.31; <3.11 ± 0.08; 2.83 ± 0.08	referred to as Nahuel Huapi Tephra by Villarosa et al. (2006)	Lara et al., 2006; Singer et al., 2008; Villarosa et al., 2006
Chaitén	Cha1	yellow pumice lapilli to coarse ash deposit (fall deposit)	medium-coarse beige ash	rhyolite (~75–76% SiO_2)	3.5*	5	5.4	NNE	400	9685–10,105	9898	125	9.91 ± 0.14; 9.92 ± 0.13; 9.87 ± 0.16; ≤10.38 ± 0.10		Watt et al., 2011; Amigo et al., 2013; Watt et al., 2015

Footnote Previous age estimates, where known, were compiled by Fontijn et al. (2014) and mostly reflect radiocarbon dates on charcoal entrained within deposits or palaeosols below/above. Previous age estimates for Mocho-Choshuenco units are modelled ages presented by Rawson et al. (2015). Magnitude estimated from deposit volume (Pyle, 2000), assuming (medial) fall deposit density of 800 kg/m^3 (pumice) or 1000 kg/m^3 (scoria), and PDC deposit density of 1500 kg/m^3. Volcanic Explosivity Index (VEI) and magnitude values in italics indicate rough estimates based on deposit thickness, in comparison with other, better-defined units. *Volume and magnitude estimates from literature (compiled by Fontijn et al., 2014; and Rawson et al., 2015).

totals between 96 and 100.5% were retained. For old silicic tephras with totals systematically around 95% as a result of devitrification, the lower threshold was set at 94% for the retention of analysis. Full results including secondary standard analyses are reported in Supplementary Table S3a,b. Table 3 presents a summary of average glass composition for key units. Fig. 2 presents a selection of variation diagrams used to discriminate units. Correlations for these units by samples and between sections are presented in Supplementary Fig. S4a–d, broken down by volcano and compositional group.

Radiocarbon dating of individual or, in some cases, several pieces of charcoal or wood entrained within pyroclastic deposits or confining soil horizons, and on organic-rich soils, was performed at the NERC Radiocarbon Facility – East Kilbride, UK. Samples were digested in 2 M HCl at 80 °C for 8 h, washed free from mineral acid with deionised water, and digested in 1 M KOH at 80 °C for 2 h. The digestion was repeated using deionised water until no further humics were extracted. The residue was rinsed free of acid, dried and homogenised. The total carbon in a known weight of pre-treated sample was recovered as CO_2 by heating with CuO in a sealed quartz tube. The gas was converted to graphite by Fe/Zn reduction and analysed by Accelerator Mass Spectroscopy. A total of 31 samples from terrestrial sections was analysed; results are reported in Table 4.

3. Tephrochronological model construction

Field, chemical and chronological data were combined to construct a regional age model of tephra deposition allowing 1) the synchronisation of terrestrial with lacustrine sections; 2) a first-order evaluation of the frequency of large explosive eruptions impacting the Chilean Lake District.

3.1. Correlations

Correlations between sections are constrained by lithological observations in the field, relative stratigraphic positions in terrestrial and lacustrine sections, and glass geochemical compositions (Fig. 3; Supplementary Fig. S4). Table 1 presents an overview of the main characteristics of the widespread marker horizons that were identified, both in lacustrine and terrestrial environments. The spatial distributions of these marker horizons are also visualised in Supplementary Information S2. Unit names were adopted from literature where possible (for a review, see Fontijn et al., 2014). Others that were, to the best of our knowledge, not described before were given a new unique name. Glass major element compositions are distinct and narrowly constrained for most widespread units. Dacitic to rhyolitic units are found for Llaima, Sollipulli, Quetrupillan, Lanín, Mocho-Choshuenco, Puyehue-Cordón Caulle and Antillanca (Table 1). Some of these were previously known from the literature, but were in some cases poorly characterised in terms of age and/or chemical composition (e.g., Llaima Pumice from Llaima volcano); others are newly described (e.g., Ranco Pumice from Puyehue-Cordón Caulle; Table 1). These silicic units tend to form regional-scale marker horizons which can be traced over at least several hundreds of km^2 and have been preserved across a range of sedimentary environments. A few more mafic units also show distinct compositions, and typically result from either unusually large eruptions (e.g., Pucón Ignimbrite and its related fall deposit from Villarrica volcano), or from scoria cones that are spatially and chemically distinct from the large volcanic centres in the area (e.g., Huanquihue, Caburgua-Huelemolle; Table 1). Accurate fingerprinting of basaltic andesitic samples using glass composition is often compromised by the abundance of microphenocrysts, which make it challenging to find glassy patches large enough to allow for EMP analysis. Moreover, where it is analytically possible to characterise basaltic andesitic samples, they often display very similar major element compositions between different units from the same frequently erupting volcano (e.g., Villarrica), or even between volcanoes (e.g., Villarrica vs. Llaima).

Lake sediment cores containing several widespread marker horizons allow the reconstruction of a relative stratigraphic sequence of large eruptions from multiple source volcanoes. The VILLAR1 core (Lago Villarrica, Fig. 1) for example, clearly demonstrates that the Llaima Pumice unit occurs stratigraphically between MC4 (Neltume Pumice) and Cha1 (Table 1; Fig. 3), which was not previously possible to resolve using radiocarbon dates on proximal deposits alone (see Fontijn et al., 2014, for a review). The relative stratigraphy constrained by VILLAR1 and other sections containing multiple marker horizons was further expanded with terrestrial sections to include all of the regionally recognised marker tephras, predominantly in the northern part of the Lake District, where the lake sections are located. Existing and new radiocarbon dates on proximal sections of these marker horizons were compiled in their relative stratigraphic order and imported into OxCal 4.2.3 (Bronk Ramsey, 2009; https://c14.arch.ox.ac.uk/oxcal/OxCal.html) for Bayesian modelling using the SHCal13 calibration curve (Hogg et al., 2013). This technique allows the estimation of a precise calibrated age of the tephra deposits, i.e. time of eruption, rather than the age of e.g., the palaeosol underneath the deposits. This calibrated eruption age can then be transferred between all sedimentary sections where the same tephra deposit is identified (e.g., Blockley et al., 2008). Only deposits which are identified in multiple localities, as verified by glass geochemistry, and that typically occur up to at least 30 km from the source volcano, were incorporated in our age model. All incorporated radiocarbon dates (84 in total, of which 3 on organic matter entrained within lacustrine sediments), including those taken from literature, are listed in the Oxcal code written out in Supplementary Information S5. The radiocarbon dates on lacustrine sediments were not corrected using the method of Bertrand et al. (2012), because no Nitrogen/Carbon measurements were made on the bulk sediments. Deposits for which no proximal radiocarbon dates were available were put in their relative stratigraphic order into the model (Supplementary Information S5), resulting in a first approximation of their absolute age (Table 1; Fig. 3). Table 1 reports the modelled age range for each deposit at the 95.4% confidence interval. For reasons of clarity, we will in the text and figures further refer to modelled ages, and also to calibrated ages from literature, by the mean $\pm 2\sigma$ cal ka BP.

3.2. Deposit volumes

After correlations were confirmed by chemical data, the deposit volumes of the most widespread and best documented deposits of Plinian-scale eruptions for which new field data were collected, were estimated using the method of Pyle (1989, 1995) using Ash-Calc (Daggitt et al., 2014, Table 1). For most of the documented units, insufficient field localities are available to estimate deposit volumes more precisely using more advanced methods (Bonadonna et al., 2015, and references therein). Hence, our estimates only reflect minimum values, as the isopachs only capture the medial parts of the deposits (Fig. 4). Tephra deposited in lakes may not represent primary fallout thickness (e.g., Bertrand et al., 2014) so was not used in these volume calculations. Where insufficient data were available to estimate minimum deposit volumes, an approximate (*minimum*) Volcanic Explosivity Index (Newhall and Self, 1982) and magnitude (Pyle, 2000) were qualitatively assigned based on the relative observed thickness compared to better described deposits in presumed downwind localities. The regionally dispersed tephra deposits typically reflect eruptions of magnitudes of at least 4.5, up to 6.2, corresponding to erupted masses of order 10^{11}–10^{13} kg (Pyle, 2000).

Table 2
Lakes and sediment cores sampled for visible tephra layers in this study.

Lake	Core ID	Lat	Long	Core type	Length (cm)	Year taken	Sampled tephra layers (*n*)	Reference
Laguna Las Ranas	LR0901B	39.189 S	72.087 W	Piston	677	2009	16	
Lago Villarrica	VILLSC01	39.281 S	72.143 W	Gravity	112	2009	1	
	VILLSC02	39.257 S	72.171 W	Gravity	81	2009	1	1
	VILL1	39.257 S	72.171 W	Piston	1374	2009	22	
	VILLAR1	39.283 S	72.210 W	Piston	800	2012	12	2
Lago Calafquen	CALA01	39.540 S	72.210 W	Gravity	123	2011	5	1
	CALA02	39.546 S	72.219°W	Gravity	104	2011	8	3; 4
	CALSC01	39.546°S	72.219°W	Gravity	106	2009	6	
	CALSC02	39.549°S	72.249°W	Gravity		2009	7	
	CAL1	39.546°S	72.219°W	Piston	880	2009	26	
	CAL2/3	39.549°S	72.250°W	Piston		2009	57	5
Lago Pullinque	PULGC01	39.571°S	72.163°W	Gravity	45	2008	1	3
Lago Panguipulli	PAGC03	39.666°S	72.275°W	Gravity	64	2008	4	3
Lago Riñihue	RINGC03	39.794°S	72.388°W	Gravity	80	2008	2	3
	RI6	39.794°S	72.388°W	Gravity	58	2011	3	4
	RIN2	39.816°S	72.389°W	Piston	727	2009	34	5
Lago Ranco	RAN3	40.183°S	72.454°W	Gravity	72	2011	13	3
Lago Maihue	MAI12	40.260 S	72.110 W	Gravity	102	2009	15	
Lago Puyehue	PUY07	40.683 S	72.419 W	Gravity	108	2011	18	3
Lago Rupanco	RUP04	40.865 S	72.495 W	Gravity	59	2009	8	3
Lago Llanquihue	LLA4	41.136 S	72.827 W	Gravity	37	2011	10	3

References: [1] Van Daele et al., 2014; [2] Wiemer et al., 2015; [3] Van Daele et al., 2015; [4] Moernaut et al., 2014; [5] Moernaut et al., 2016.

4. Discussion

4.1. Age estimates for major eruptions

Our tephrochronological model for the Lake District is schematically presented in Fig. 5, depicting the modelled age distribution, approximate magnitude and composition (average SiO_2 content) of each unit. The regional marker horizons in the area are now described by one single precisely constrained age, rather than a set of radiocarbon dates acquired from charcoal entrained within the deposits or their enclosing palaeosol horizons. Unsurprisingly, most modelled ages of previously well documented deposits are consistent with their previously published radiocarbon ages (e.g., Alpehue Pumice: 2.93 ± 0.18 to 2.99 ± 0.18 cal ka BP, after Naranjo et al., 1993; modelled age 2.95 ± 0.11 cal ka BP, Table 1). The modelled ages of some other units which previously had only poor age constraints now have significantly improved precision, facilitating their use as time markers in different sedimentary archives. This particularly applies to the Llaima Pumice, with previous radiocarbon dates varying between 8.20 ± 0.34 cal ka BP and 10.12 ± 0.20 cal ka BP (Fontijn et al., 2014), and which now has a modelled age of 10.45 ± 0.13 cal ka BP (Table 1).

Our model provides the first age estimates for a number of eruptions from basaltic cones which appear spatially unrelated to the large edifice volcanoes. The VILLAR1 and LR0901B cores (Table 2) both show two basaltic tephra layers with compositions strongly resembling those of terrestrial samples taken from Strombolian-style scoria fall deposits near the heavily vegetated Caburgua-Huelemolle scoria cones, ca. 25–30 km NE of Villarrica volcano (Fig. 1). The two lacustrine layers both occur stratigraphically between Cha1 and Llaima Pumice (Fig. 3), and are interpreted to represent two single eruptions in a relatively narrow timeframe, over the course of approximately 1–2 centuries, from the same basaltic cone field. Because it is not possible to assign a specific cone source to either of the deposits, and because they occur temporally close to each other, we considered them as a single event in our chronological model (CabHuel, 10.38 ± 0.09 cal ka BP; Table 1).

Another tephra deposit identified in the lake cores, HUA1, has a modelled age of 4.12 ± 0.09 cal ka BP. Its composition is virtually indistinguishable from that of the distinct 359 ± 10 varve yr BP tephra layer that was linked to the Achen Ñihue eruption of the Huanquihue Group (Fig. 1), and which is a useful marker horizon in many of the short sediment cores in the Lake District (Van Daele et al., 2014). The HUA1 tephra shows that the Huanquihue Group, thought to be mostly of Pleistocene age, with a Holocene compound cinder cone (Siebert et al., 2010; Global Volcanism Program, http://volcano.si.edu), has been active throughout the mid-late Holocene at least.

4.2. Tephrochronological markers

The most important marker horizons which are widespread over the Lake District and especially easily identifiable in the sediments of the studied lakes, are MC4 (Neltume Pumice from Mocho-Choshuenco, 11.40 ± 0.81 cal ka BP), Cha1 (Chaitén, 9.90 ± 0.25 cal ka BP), Ranco Pumice (Puyehue-Cordón Caulle, 4.35 ± 0.33 cal ka BP), Mil Hojas (Puyehue-Cordón Caulle, 0.84 ± 0.18 cal ka BP), and Achen Ñihue (Huanquihue Group, 0.36 ± 0.01 cal ka BP; Fig 4; Supplementary Information S2). Thanks to a partly northward distribution, these horizons enable synchronisation of sedimentary records on a regional scale, spanning most of the postglacial period. Other major units (e.g., Alpehue Pumice, Llaima Pumice, PCC2; Table 1; Fig. 4) were preferentially dispersed to the east and are typically only identified in one lacustrine archive, in addition to terrestrial sections. These units therefore may have a higher potential as marker horizons in Argentinian lakes. Nevertheless, within the Chilean Lake District they are still identified onshore over distances typically several tens of kms from source.

We anticipate that a number of tephra layers that have previously been identified, but not chemically characterised for glass composition, in the sediments of Laguna El Trébol (~41.1°S; Tatur et al., 2002), Lago Mascardi (~41.3°S; Massaferro and Corley, 1998; Román-Ross et al., 2002) and Lagunas Huala Hué and Padre Laguna (~41.4°S; Iglesias et al., 2012, Fig. 1) will correspond to units presented here, especially those sourced from Puyehue-Cordón Caulle and Antillanca volcanoes (Table 1). Indeed, Villarosa et al. (2006) interpreted one of the deposits found in the sediments of Laguna El Trébol and surrounding areas as the Nahuel Huapi Tephra (NHT), mainly based on its physical appearance (white pumice capped by dark brown scoria). Our age modelling suggests the age

Table 3
Average and standard deviation (italics) of glass major element composition of widespread marker tephras analysed in this study. Full dataset, including secondary glass standards, are presented in Supplementary Table S3a,b.

Volcano	Unit		Point	SiO_2	TiO_2	Al_2O_3	FeO	MnO	MgO	CaO	Na_2O	K_2O	P_2O_5	Cl	Tot
Llaima	Llaima Pumice -pumice	n = 31	avg	69.09	0.44	15.55	3.93	0.15	0.51	2.44	6.11	1.65	0.12		98.45
			sd	*1.32*	*0.10*	*1.03*	*0.58*	*0.04*	*0.16*	*0.66*	*0.22*	*0.27*	*0.04*		*1.28*
Llaima	Llaima Pumice – scoria	n = 40	avg	61.05	1.26	16.19	7.23	0.19	2.16	5.18	5.22	1.14	0.38		98.96
			sd	*0.72*	*0.11*	*0.73*	*0.54*	*0.06*	*0.25*	*0.39*	*0.21*	*0.12*	*0.04*		*1.06*
Sollipulli	Alpehue Pumice	n = 63	avg	73.84	0.26	14.07	1.73	0.04	0.21	1.03	4.61	4.17	0.03		98.48
			sd	*0.42*	*0.03*	*0.22*	*0.14*	*0.03*	*0.03*	*0.11*	*0.36*	*0.11*	*0.02*		*1.42*
Caburgua Huelemolle	CabHuel	n = 106	avg	53.77	1.83	14.68	10.80	0.20	4.83	8.41	3.68	1.34	0.47		98.93
			sd	*0.94*	*0.16*	*0.71*	*0.73*	*0.05*	*0.55*	*0.58*	*0.31*	*0.37*	*0.13*		*0.70*
Villarrica	Chaimilla	n = 46	avg	55.85	1.38	15.27	9.82	0.18	4.59	8.51	3.33	0.82	0.25		99.23
			sd	*0.56*	*0.14*	*1.47*	*1.00*	*0.04*	*0.78*	*0.45*	*0.33*	*0.09*	*0.04*		*0.65*
Villarrica	Pucón Ignimbrite	n = 285	avg	57.37	1.40	15.60	9.71	0.18	3.58	7.25	3.62	1.02	0.27	0.07	99.06
			sd	*0.71*	*0.11*	*0.71*	*0.53*	*0.05*	*0.35*	*0.40*	*0.36*	*0.12*	*0.04*	*0.02*	*0.97*
Villarrica	Licán Ignimbrite	n = 4	avg	58.82	1.34	15.91	9.46	0.18	2.73	6.30	3.90	1.08	0.27		99.76
			sd	*1.15*	*0.06*	*1.10*	*0.64*	*0.05*	*0.60*	*0.36*	*0.19*	*0.06*	*0.02*		*0.80*
Quetrupillan	Quet5	n = 97	avg	66.89	0.99	15.63	4.39	0.12	1.11	2.86	4.52	3.22	0.27	0.13	98.48
			sd	*0.43*	*0.08*	*0.18*	*0.27*	*0.07*	*0.09*	*0.14*	*0.20*	*0.10*	*0.04*	*0.03*	*0.68*
Quetrupillan	Puesco	n = 483	avg	67.70	0.89	15.36	4.07	0.12	0.92	2.49	4.81	3.43	0.22	0.14	98.74
			sd	*0.45*	*0.08*	*0.18*	*0.22*	*0.06*	*0.07*	*0.12*	*0.37*	*0.11*	*0.03*	*0.04*	*1.27*
Quetrupillan	Quet3	n = 86	avg	69.26	0.75	15.31	3.53	0.10	0.81	2.23	4.70	3.17	0.15	0.16	99.08
			sd	*0.78*	*0.08*	*0.34*	*0.46*	*0.07*	*0.17*	*0.34*	*0.29*	*0.30*	*0.04*	*0.03*	*0.98*
Quetrupillan	Quet2	n = 49	avg	70.17	0.58	15.30	2.75	0.08	0.62	1.87	5.08	3.44	0.11	0.20	98.28
			sd	*0.73*	*0.07*	*0.41*	*0.28*	*0.04*	*0.13*	*0.24*	*0.50*	*0.15*	*0.03*	*0.04*	*1.22*
Quetrupillan	Quet1	n = 113	avg	72.05	0.42	14.83	2.22	0.08	0.37	1.29	4.81	3.87	0.06	0.19	97.98
			sd	*0.45*	*0.05*	*0.30*	*0.17*	*0.06*	*0.03*	*0.18*	*0.23*	*0.14*	*0.03*	*0.04*	*1.34*
Huanquihue Group	Achen Ñihue	n = 127	avg	54.00	2.18	14.60	12.38	0.25	3.30	6.83	4.00	1.90	0.56	0.13	98.48
			sd	*0.97*	*0.14*	*0.60*	*0.77*	*0.05*	*0.41*	*0.28*	*0.32*	*0.22*	*0.05*	*0.02*	*0.86*
Huanquihue Group	HUA1	n = 48	avg	54.07	2.18	13.90	12.93	0.25	3.50	6.97	3.96	1.77	0.47	0.11	98.01
			sd	*0.59*	*0.09*	*0.32*	*0.56*	*0.05*	*0.43*	*0.36*	*0.30*	*0.29*	*0.04*	*0.02*	*0.65*
Mocho-Choshuenco	MC23	n = 147	avg	59.30	1.41	15.79	8.41	0.19	2.79	5.78	4.75	1.25	0.33		98.83
			sd	*0.33*	*0.06*	*0.25*	*0.28*	*0.04*	*0.11*	*0.16*	*0.20*	*0.06*	*0.02*		*0.83*
Mocho-Choshuenco	MC18	n = 20	avg	62.52	1.20	16.15	6.34	0.16	1.89	4.65	5.26	1.46	0.38	0.10	98.64
			sd	*0.65*	*0.18*	*0.74*	*0.87*	*0.04*	*0.27*	*0.30*	*0.30*	*0.17*	*0.02*	*0.02*	*1.00*
Mocho-Choshuenco	MC15	n = 49	avg	60.87	1.37	16.03	7.43	0.19	2.35	5.18	4.70	1.50	0.37	0.11	98.66
			sd	*0.59*	*0.09*	*0.66*	*0.65*	*0.04*	*0.38*	*0.24*	*0.35*	*0.13*	*0.03*	*0.02*	*0.98*
Mocho-Choshuenco	MC4	n = 206	avg	70.24	0.56	15.47	2.92	0.12	0.61	2.17	5.37	2.39	0.14	0.16	97.50
			sd	*1.75*	*0.15*	*0.77*	*0.62*	*0.06*	*0.30*	*0.67*	*0.52*	*0.25*	*0.09*	*0.03*	*1.43*
Puyehue-Cordón Caulle	Mil Hojas	n = 406	avg	70.01	0.67	14.31	4.01	0.12	0.58	2.11	5.22	2.84	0.13	0.20	98.61
			sd	*0.54*	*0.06*	*0.25*	*0.21*	*0.04*	*0.07*	*0.17*	*0.29*	*0.16*	*0.03*	*0.02*	*0.83*
Puyehue-Cordón Caulle	PCC4	n = 43	avg	67.68	0.93	14.37	5.36	0.16	0.90	2.89	4.99	2.46	0.26	0.16	99.00
			sd	*0.28*	*0.05*	*0.31*	*0.18*	*0.04*	*0.07*	*0.14*	*0.20*	*0.09*	*0.02*	*0.02*	*1.16*
Puyehue-Cordón Caulle	Ranco	n = 239	avg	71.54	0.35	14.10	3.79	0.13	0.26	1.67	5.19	2.92	0.06	0.21	98.61
			sd	*0.62*	*0.07*	*0.28*	*0.27*	*0.04*	*0.07*	*0.17*	*0.31*	*0.10*	*0.03*	*0.03*	*0.89*
Puyehue-Cordón Caulle	PCC2	n = 108	avg	72.58	0.29	13.93	3.14	0.11	0.18	1.46	5.20	3.08	0.04	0.18	98.12
			sd	*0.58*	*0.04*	*0.32*	*0.28*	*0.03*	*0.06*	*0.17*	*0.24*	*0.14*	*0.02*	*0.01*	*0.99*
Puyehue-Cordón Caulle	PCC1	n = 59	avg	70.15	0.47	14.22	4.49	0.16	0.36	2.07	5.23	2.76	0.09		98.78
			sd	*0.42*	*0.06*	*0.14*	*0.21*	*0.03*	*0.07*	*0.12*	*0.16*	*0.08*	*0.03*		*0.74*
Antillanca Group	Rayhuen	n = 18	avg	63.29	0.98	16.29	5.91	0.16	1.94	4.42	4.88	1.79	0.34	0.16	98.85
			sd	*0.82*	*0.08*	*0.63*	*0.50*	*0.04*	*0.50*	*0.44*	*0.66*	*0.20*	*0.03*	*0.01*	*0.88*
Antillanca Group	NHT	n = 67	avg	72.07	0.36	15.01	2.05	0.09	0.54	2.10	4.87	2.82	0.09		98.08
			sd	*0.62*	*0.06*	*0.30*	*0.33*	*0.04*	*0.06*	*0.17*	*0.19*	*0.11*	*0.03*		*0.91*
Chaitén	Cha1	n = 71	avg	76.06	0.11	13.86	1.32	0.06	0.20	1.22	3.98	3.12	0.07		95.32
			sd	*0.50*	*0.03*	*0.28*	*0.12*	*0.03*	*0.04*	*0.12*	*0.31*	*0.11*	*0.03*		*1.14*

of the NHT, here referred to as Playas Blancas Negras (PBN), to be 2.24 ± 0.04 cal ka BP (Table 1). The Mascardi, Huala Hué and Padre Laguna records all show at least one potential correlative tephra layer with PBN, roughly within the 2–2.5 ka timeframe (Iglesias et al., 2012; Massaferro and Corley, 1998). The same records also all show distinct tephra horizons in the mid-Holocene (ca. 4–4.5 ka; Iglesias et al., 2012; Massaferro and Corley, 1998). Based on their stratigraphic position, some of these tephra horizons may therefore correspond to our Ranco Pumice (4.35 ± 0.33 cal ka BP; Table 1) from Puyehue-Cordón Caulle. Another likely candidate to be found in the sedimentary archives around 41–41.5°S is Cha1, given its northward dispersal (Watt et al., 2015). Tatur et al. (2002) describe a number of white and grey tephra layers around approximately 10 cal ka BP, which could potentially correspond to Cha1. Also in the Laguna Huala Hué core, a number of whitish tephra layers are identified in the early Holocene (Iglesias et al., 2012), all of which could correspond to Cha1. Without chemical characterisation of the major element glass composition by EMP, which is increasingly the favoured approach in tephrochronology (e.g., Kuehn et al., 2011; Pearce et al., 2014), none of these correlations can however be confirmed. The Laguna El Trébol record holds more than 50 tephra deposits, spanning the last ~15 kyr, but its age model is only poorly constrained, with radiocarbon ages mostly concentrated around the Late Pleistocene–Holocene transition. Villarosa et al. (2006) suggest a few correlations between the El Trébol record and surrounding sites (mostly caves) based on additional radiocarbon dates and physical appearance of tephra (e.g., colour) but these correlations are not supported by geochemical data. Considering the vast number of tephra layers in the El Trébol record, correlations which are not verified by glass geochemistry should be treated with great caution. Positive correlations with PBN, Ranco Pumice, Cha1, or indeed other tephra deposits between the

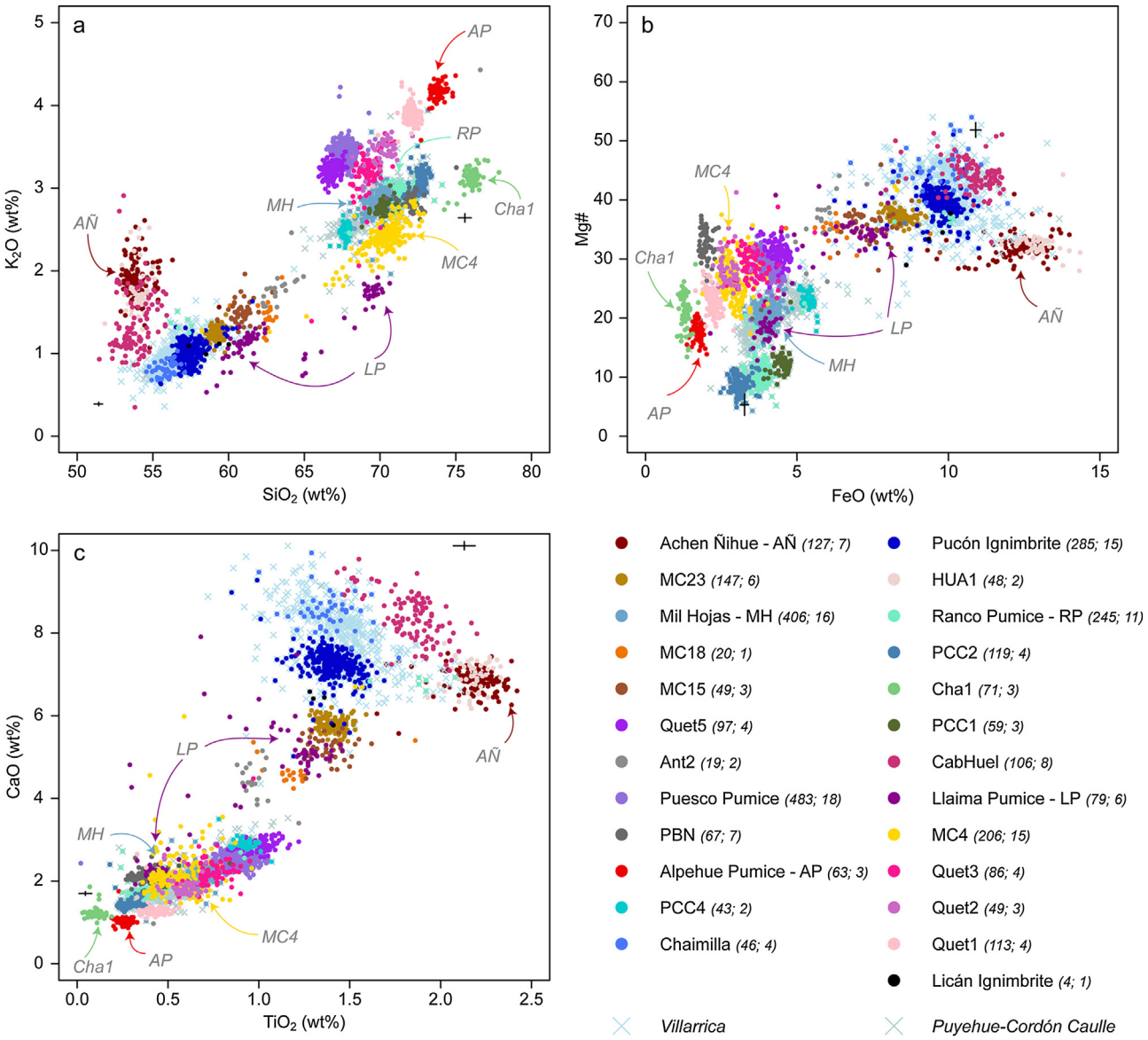

Fig. 2. Selection of variation diagrams illustrating correlations between units based on glass major element composition. (a) K_2O vs. SiO_2; (b) Mg# vs. FeO, with [Mg# = 100* Mg/(Mg + Fe)]; (c) CaO vs. TiO_2. Each symbol represents an individual analysis. Crosses for Villarrica and Puyehue-Cordón Caulle indicate all analyses of samples linked to either volcano but which could not be correlated to a specific unit. Correlated units are sorted by age, Achen Ñihue being the youngest and Licán Ignimbrite being the oldest (Table 1). Numbers in parentheses indicate total amount of individual analyses, and amount of samples analysed. Symbol colours correspond to correlated units illustrated in Fig. 3. Black crosses indicate error bars calculated for the ML3B-G and ATHO-G secondary standards (Jochum et al., 2006) averaged for all analytical runs (Supplementary Table S3b), and are placed at the preferred values of these standards, except in (c), where they were moved within the plot field (ML3B-G) and outside the cluster of data points (ATHO-G). Supplementary Fig. S4 represent similar plots, broken down by sample and volcano. (For interpretation of the references to colour in this figure legend, the reader is referred to the web version of this article.)

different sedimentary archives in the area, would enable palaeoenvironmentalists to constrain the precise timing of changes in the vegetation cover in the area (e.g., Iglesias et al., 2012) and other palaeoecological proxies (e.g., Massaferro and Corley, 1998) in response to climatological conditions, and more accurately correlate multiple records.

4.3. Extending the regional tephra records

The tephrochronological framework developed here significantly improves our understanding of the timing of large explosive events impacting the Chilean and Argentinian Lake District throughout the postglacial. Fig. 6 schematically illustrates how this record for the Lake District (ca. 38 to 42°S) can potentially be extended and integrated with tephrochronological records further south into Patagonia, and used to synchronise various palaeoenvironmental records.

We tentatively suggest a correlation of the Mil Hojas deposits (Table 1) between our new records from Lago Villarrica, Lago Calafquen and Lago Riñihue, and those of Lago Puyehue at 40.7°S (Bertrand et al., 2008b). Other Puyehue-Cordón Caulle units are less straightforward to integrate with the Lago Puyehue record using the existing dataset. This is partly due to the wealth of tephra layers that exist in the Lago Puyehue core and the fact that most of them have not been chemically analysed (at least 78 visible tephras in the last 14 ky, with several probably still unaccounted for; Bertrand et al., 2008b). The identification of 2011 Cordón Caulle tephra in Lago Puyehue's sediments, despite a strong eastward dispersal and

Table 4
New Accelerator Mass Spectroscopy radiocarbon dates on terrestrial samples obtained for this study, performed at the NERC Radiocarbon Facility – East Kilbride. Calibrations were performed in Oxcal 4.2 (Bronk Ramsey, 2009) using the SHCal13 calibration curve (Hogg et al., 2013), and represent the 95.4% probability range. Unit of interest indicated for each sample: those indicated in bold were taken up in our tephrochronological model. Other units were not widespread enough to be useful marker horizons. In addition to our new dates on terrestrial samples, we also list three radiocarbon dates on charcoal and wood fragments encountered underneath tephra deposits within sediment core LR0901B (Table 2; acquired by Abarzúa et al., unpublished data), and which were used in our regional age model reconstruction.

Sample ID	Lab code	Latitude (°S)	Longitude (°W)	$\delta^{13}C$‰ (±0.1)	Conventional age (^{14}C yr BP)	+/− 1σ (^{14}C yr BP)	Calibrated age range (cal yr BP)	Probability %	Calibrated age (cal ka BP) mean	+/− 1σ (cal ka BP)	Sample type	Stratigraphic position	Unit of interest (Volcano)
CLD026B	SUERC-56143	−39.312	−71.979	−26.3*	3882	38	4411–4147 4115–4100	93.1 2.3	4.257	0.081	charcoal	entrained within PDC base	**Pucón Ignimbrite (Villarrica)**
CLD030B	SUERC-56144	−39.437	−71.790	−24.6	3787	36	4236–3980	95.4	4.098	0.072	charcoal	entrained within PDC deposit	**Pucón Ignimbrite (Villarrica)**
CLD041A	SUERC-56145	−39.451	−71.551	−26.9	3848	38	4405–4367 4357–4323 4317–4083 4025–4013	4.0 4.4 86.1 0.9	4.201	0.082	charred wood	soil under bedded ash fall deposits	Huililco deposits (Quetrupillan)
CLD064A	SUERC-56148	−39.068	−71.515	−22.2	2958	35	3206–3200 3180–2944 2932–2930	0.4 94.8 0.2	3.059	0.066	charcoal	entrained within PDC deposit	**Alpehue Pumice (Sollipulli)**
CLD154F	SUERC-56149	−40.210	−71.947	−30.8	3820	43	4350–4331 4297–3983	1.3 94.1	4.155	0.086	charcoal	soil above pumice fall deposit	**Ranco Pumice (PCC)**
CLD154G	SUERC-56150	−40.210	−71.947	−27.0	4166	35	4821–4527	95.4	4.668	0.089	charcoal	soil under pumice fall deposit	**Ranco Pumice (PCC)**
CLD160D	SUERC-56151	−39.458	−71.816	−25.1	3622	41	4064–4047 3987–3720	1.4 94.0	3.879	0.073	charcoal	soil under PDC/scoria fall deposit	**Pucón Ignimbrite (Villarrica)**
CLD160J	SUERC-56152	−39.458	−71.816	−25.4	5765	38	6635–6413	95.4	6.521	0.061	charred wood	entrained within PDC deposit	(Villarrica)
CLD164B	SUERC-56153	−39.554	−71.537	−27.1	2012	35	2004–1863 1857–1837	90.0 5.4	1.930	0.045	charcoal	soil under pumice fall deposit	**Puesco Pumice (Quetrupillan)**
CLD166A	SUERC-56154	−39.525	−71.552	−27.0	2442	37	2699–2632 2617–2587 2570–2565 2540–2342	14.2 4.9 0.3 75.9	2.472	0.102	charcoal	soil under pumice fall deposit	**Puesco Pumice (Quetrupillan)**
CLD167B	SUERC-56874	−39.504	−71.545	−26.0	2171	35	2303–2241 2181–2009	15.1 80.3	2.130	0.076	charcoal	soil under pumice fall deposit	**Puesco Pumice (Quetrupillan)**
CLD167F	SUERC-56875	−39.504	−71.545	−26.6	3827	37	4350–4331 4297–4066 4047–3988	1.3 86.3 7.8	4.165	0.078	charcoal	soil under scoria fall deposit	**Pucón Ignimbrite (Villarrica)**
CLD168A	SUERC-56876	−39.503	−71.546	−26.5	233	37	315–240 230–138 114–103 94–70 23–…	29.5 59.6 1.3 2.6 2.5	0.204	0.068	charcoal	soil under top (reworked?) pumice deposit	(Quetrupillan)
CLD168K	SUERC-56877	−39.503	−71.546	−25.5	10,190	54	12,024–11,598 11,554–11,476 11,435–11,409	89.6 4.5 1.3	11.781	0.139	charcoal	soil under coarse ash deposit	**MC4 – Neltume Pumice (MC)**
CLD168O	SUERC-56878	−39.503	−71.546	−25.4	10,515	43	12,558–12,365 12,343–12,263 12,230–12,091	63.7 12.9 18.8	12.387	0.137	charcoal	soil above coarse ash deposit	**Quet1 (Quetrupillan)**
CLD177A	SUERC-56879	−39.495	−71.548	−27.5	2088	37	2145–2130 2104–1916	2.0 93.4	2.012	0.056	charred wood	soil under pumice fall deposit	**Puesco Pumice (Quetrupillan)**

(*continued on next page*)

Table 4 (*continued*)

Sample ID	Lab code	Latitude (°S)	Longitude (°W)	$\delta^{13}C$‰ (±0.1)	Conventional age (^{14}C yr BP)	+/− 1σ (^{14}C yr BP)	Calibrated age range (cal yr BP)	Probability %	Calibrated age (cal ka BP) mean	+/− 1σ (cal ka BP)	Sample type	Stratigraphic position	Unit of interest (Volcano)
CLD177C	SUERC-56880	−39.495	−71.548	−26.6	1860	37	1866–1856 1838–1696 1659–1614	0.9 86.8 7.8	1.753	0.054	charcoal	soil under pumice fall deposit	**Quet5 (Quetrupillan)**
CLD179B	SUERC-57432	−39.476	−71.550	−26.9	1956	35	1990–1970 1932–1780 1775–1745	2.6 84.8 8.0	1.859	0.050	charcoal	soil between pumice fall deposits	**Quet5/Puesco Pumice (Quetrupillan)**
CLD230B	SUERC-56883	−39.756	−71.409	−26.6	4388	38	5039–4995 4984–4840	9.7 85.7	4.926	0.061	soil with charcoal	soil under bedded ash fall deposits	(Lanín?)
CLD235A	SUERC-56885	−39.572	−71.438	−25.5	5020	36	5886–5821 5760–5603	14.3 81.1	5.716	0.069	charred wood	soil under pumice fall deposit	(Lanín?)
CLD238L	SUERC-57435	−40.700	−71.780	−26.5*	2266	37	2339–2152	95.4	2.236	0.056	soil with charcoal	soil under pumice fall deposit	**PBN (Antillanca)**
CLD244B	SUERC-56886	−40.477	−71.628	−25.9	2272	37	2338–2155	95.4	2.239	0.056	charcoal	soil under pumice fall deposit	**PBN (Antillanca)**
CLD244D	SUERC-56887	−40.477	−71.628	−26.9	5946	39	6855–6636	95.4	6.727	0.054	charcoal	soil under pumice fall deposit	**PCC2 (PCC)**
CLD246B	SUERC-56888	−40.545	−71.651	−25.7	1952	37	1986–1975 1930–1744	1.5 93.9	1.854	0.053	charcoal	soil under pumice fall deposit	**Rayhuen (Antillanca)**
CLD247C	SUERC-57436	−40.590	−71.655	−26.1	5975	39	6881–6868 6862–6664	2.2 93.2	6.760	0.058	charcoal	soil under ash/pumice deposit	**PCC2 (PCC)**
CLD248E	SUERC-56889	−40.597	−71.649	−28.0	2144	35	2299–2258 2159–1999	4.9 90.5	2.089	0.065	charcoal	soil under pumice fall deposit	**PBN (Antillanca)**
CLD248G	SUERC-56890	−40.597	−71.649	−24.4	1074	37	1053–1020 988–900 870–806	5.8 76.0 13.6	0.933	0.049	charcoal	soil under pumice fall deposit	**Mil Hojas (PCC)**
CLD249B	SUERC-56893	−40.617	−71.670	−24.5	5543	38	6400–6264 6250–6211	81.5 13.9	6.305	0.050	charcoal	soil under pumice fall deposit	**Ranco Pumice (PCC)**
CLD296F	SUERC-55750	−38.896	−71.531	−26.7	9385	41	10,692–10,420	95.4	10.557	0.071	charred wood	soil under pumice fall deposit	**Llaima Pumice (Llaima)**
CLD314C	SUERC-55751	−40.317	−71.981	−26.8	278	37	443–367 331–271 219–150	17.6 47.0 30.8	0.282	0.084	charcoal	soil under bedded ash fall deposits	(CLV)
CLD329C	SUERC-55752	−40.892	−72.308	−27.5	1523	35	1429–1301	95.4	1.363	0.037	charcoal	soil under ash/pumice deposit	(Osorno?)
LR0901B-T4-36		−39.180	−72.080	−32.7	3670	20	4073–4041 3993–3849	7.3 88.1	3.942	0.050	charcoal, twigs	under tephra deposit	**Pucón Ignimbrite (Villarrica)**
LR0901B-T6-50		−39.180	−72.080	−28.5	8910	65	10,187–9730 9723–9705	93.8 1.6	9.966	0.136	charcoal	under tephra deposit	**Cha1 (Chaitén)**
LR0901B-T7-43		−39.180	−72.080	−38.1	11,600	85	13,566–13,223	95.4	13.388	0.086	wood	under tephra deposit	**MC4 – Neltume Pumice (MC)**

*Estimated $\delta^{13}C$ values (used to correct for natural isotopic variation) due to insufficient material for an independent measurement. PDC: pyroclastic density current; PCC: Puyehue-Cordón Caulle; MC: Mocho-Choshuenco; PBN: Playas Blancas Negras; CLV: Carrán-Los Venados.

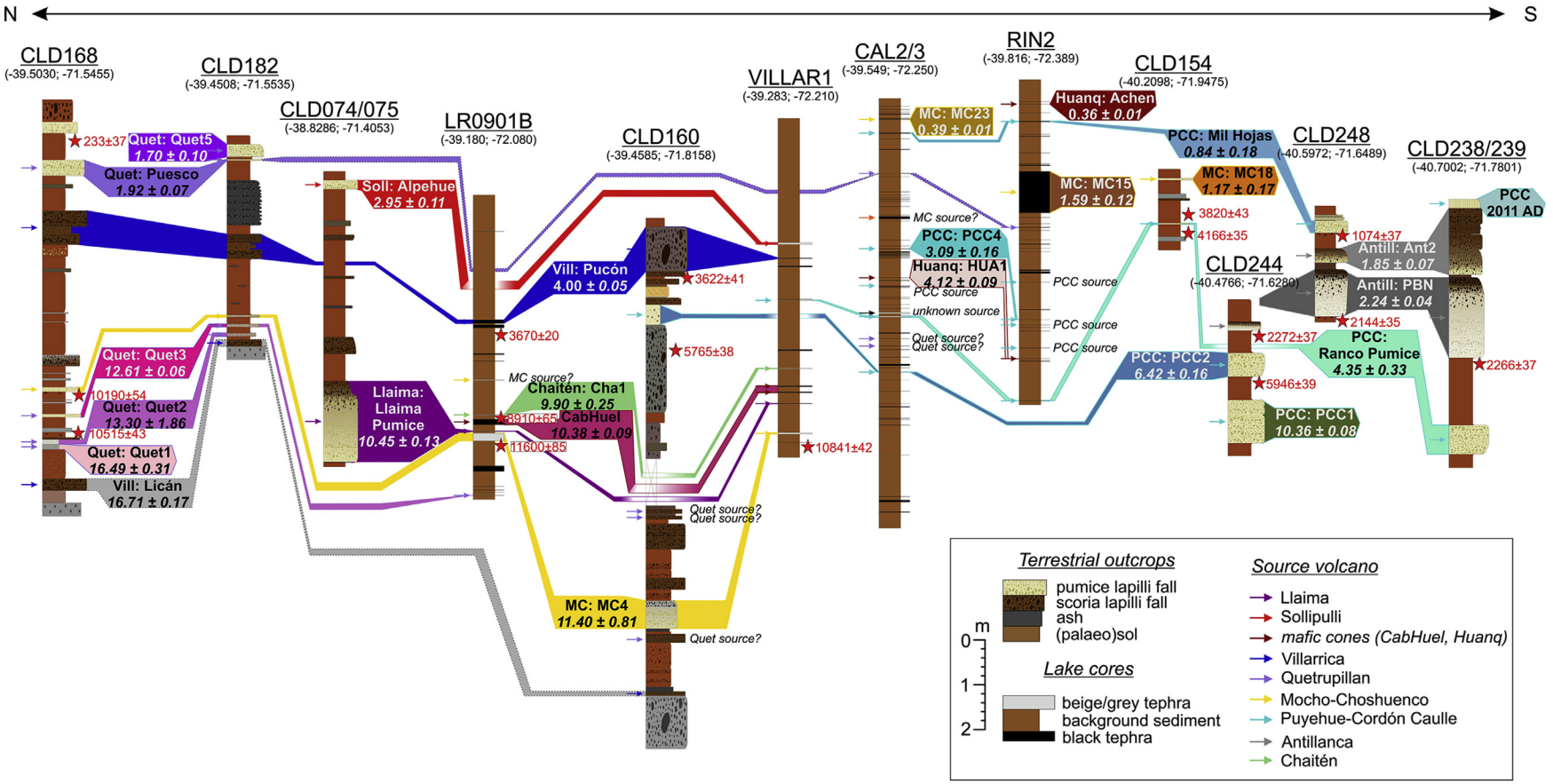

Fig. 3. Schematic representation of correlations between key terrestrial and lacustrine sections verified by relative stratigraphy and glass geochemistry. Section names starting with "CLD" are terrestrial; others are lacustrine. Sections are represented by green symbols in Fig. 1, and roughly follow a N–S transect. Coordinates are given in Latitude–Longitude using the WGS84 datum. Two correlations are less well supported by geochemistry, either due to alteration or an abundance of microphenocrysts in the samples, and are marked by dotted lines (Puesco Pumice between terrestrial and lacustrine sections; Licán Ignimbrite). Red stars indicate uncalibrated radiocarbon dates, reported in ^{14}C yr BP ± 1σ, mostly on pieces of charcoal. Unit ages are modelled ages at the 95.4% confidence level, and expressed in mean ± 2σ cal ka BP (Table 1). More information on radiocarbon dates from terrestrial sections and modelled ages are presented in Table 4. Dates from LR0901B core from Abarzúa et al. (unpublished data; Table 4), date from VILLAR1 core after Wiemer et al. (2015). Colours of correlation bars correspond to those in Fig. 2. (For interpretation of the references to colour in this figure legend, the reader is referred to the web version of this article.)

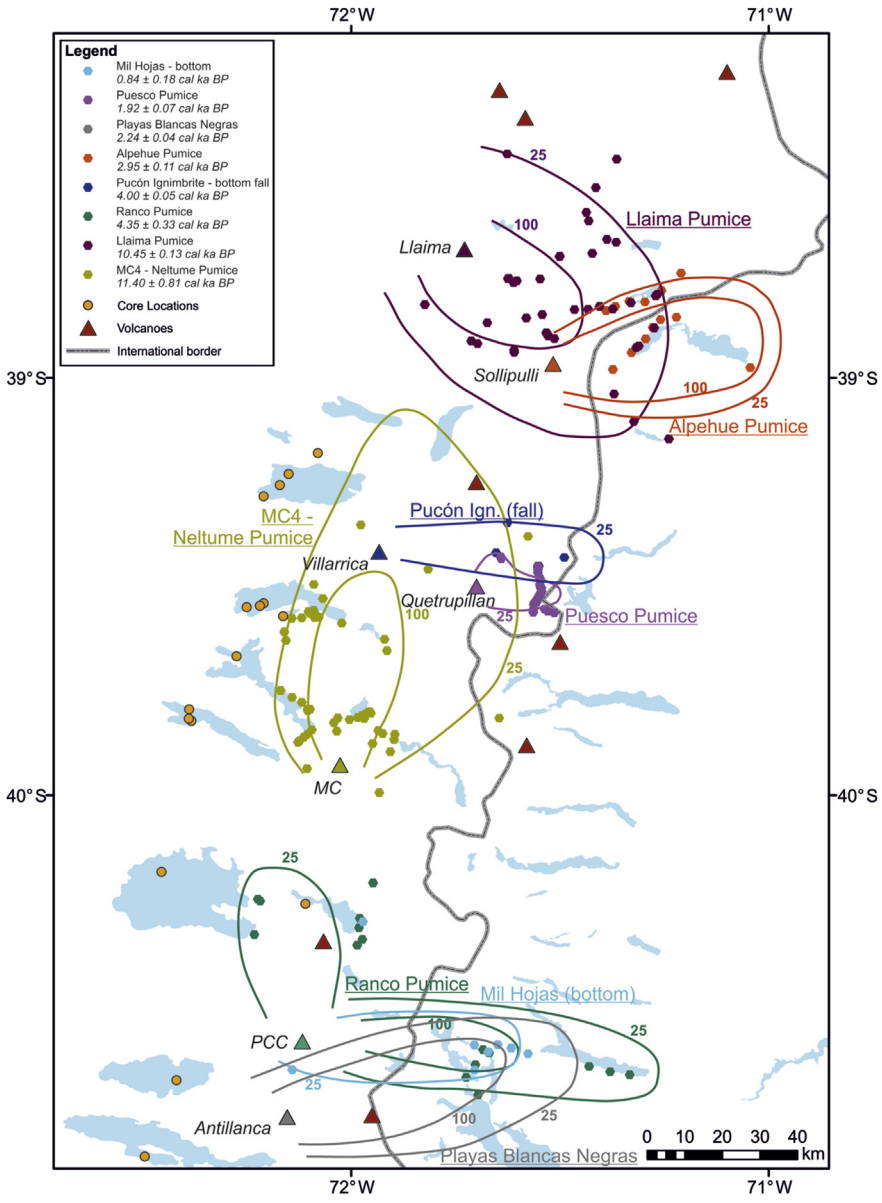

Fig. 4. Spatial dispersal, illustrated by 100 and 25 cm isopach contours, of largest described units incorporated in our age model, and originating from Lake District volcanoes (i.e. excluding Cha1, Table 1). Most of these units are preserved in the long sediment cores of Lago Villarrica and Laguna Las Ranas (Fig. 1), including units which are predominantly dispersed to the east. MC: Mocho-Choshuenco; PCC: Puyehue-Cordón Caulle.

no direct fallout over the lake (e.g., Pistolesi et al., 2015), was attributed by Bertrand et al. (2014) to transport of the tephra by rivers into the lake, and further distribution and deposition controlled by lake currents. Although the distribution of the tephra in the lake sediments does not reflect primary depositional thickness or grain size distribution in this case, it does suggest that the lake sediments can still record the occurrence of a single eruptive event if its tephra is deposited within the river catchment of the lake (Bertrand et al., 2014). It is therefore plausible that many of the thin and fine-grained layers (other than the 78 visible tephras) preserved in the Lago Puyehue sedimentary records also represent moderate-sized eruptions of Puyehue-Cordón Caulle, like the 2011 event. Bertrand et al. (2014) concluded that lakes with relatively large catchment areas, like Lago Puyehue, are clearly more sensitive to tephra input via river transport, possibly in addition to primary fallout, than lakes with small catchment areas, which tend to record primary fallout only. Lakes with large catchments, like most of the ones studied here (Fig. 1), may therefore provide the most complete tephrostratigraphic records in terms of recording individual events, even if not resulting from primary fallout. This was demonstrated by Van Daele et al. (2014) who were able to reconstruct a 600-year record of volcanic activity at Villarrica, based on the recognition of lahar deposits in the sediments of Lago Villarrica and Lago Calafquen. The record presented by Van Daele et al. (2014) is significantly more complete than that previously known from historical documents alone. Apart from the Las Ranas core, all sediment cores studied here are from lakes with large catchments (Fig. 1). The cores were taken in distal, relatively shallow sub-basins, where sandy washed-in tephras are unlikely to be incorporated into the sediments. It is possible that some very fine-grained tephras in the cores result from secondary mobilisation (Bertrand et al., 2014), though we focused our sampling predominantly on the coarser visible tephras. We are thus confident that the far majority of analysed tephras results from primary fallout. This is also consistent with most tephras showing tightly clustered geochemical compositions.

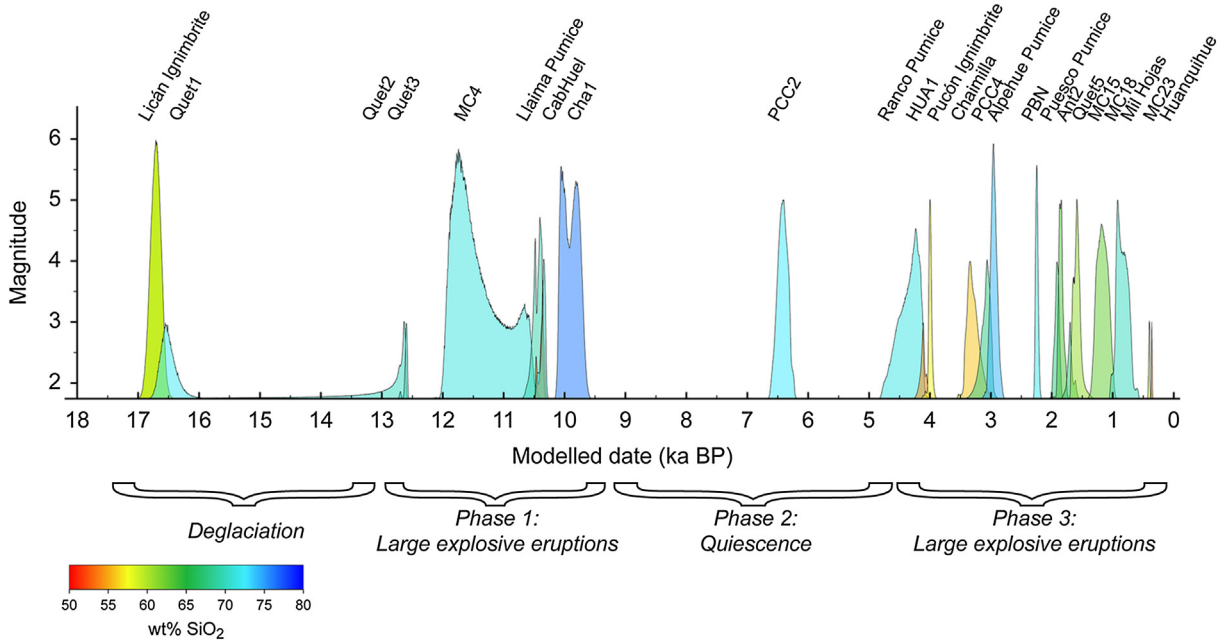

Fig. 5. Schematic representation of our tephrochronological model for the Chilean Lake District. Each unit is represented by its modelled age probability distribution: narrower distributions represent better constrained (i.e. more precise) modelled ages. Unit age distributions are colour-coded by the average SiO_2 content of the glass: most regionally dispersed units are dacitic to rhyolitic in composition. Peaks are scaled by the approximate magnitude of the deposit they represent: higher peaks represent larger eruptions. The temporal spacing of marker horizons in the Lake District is seemingly skewed towards the earlier postglacial (~17–9.5 ka; McCulloch et al., 2000) and the last 4.5 kyr. (For interpretation of the references to colour in this figure legend, the reader is referred to the web version of this article.)

Moreno et al. (2015a) recently described a sediment record of Lago Teo, ca. 8.5 km SW of Chaitén volcano (Fig. 1), which holds multiple tephra deposits with a rhyolitic composition very similar to that of the Cha1 and Chaitén 2008 deposits. As was already indicated by Amigo et al. (2013) and Watt et al. (2013b), the record suggests that Chaitén has been much more active throughout the Holocene than had previously been thought (e.g. Naranjo and Stern, 2004). From a comparison of the stratigraphic and geochronological information, and published geochemical data, we tentatively suggest that the mid-Holocene Cha2 deposit (Watt et al., 2013b) corresponds to LLT-12 of Moreno et al. (2015a), and that the "rhyolite between Cha1 and Cha2" of Amigo et al. (2013), or ChaA1 (Fontijn et al., 2014), corresponds to LLT-17 of Moreno et al. (2015a). Chemical data presented by Bertrand et al. (2008b) on horizon PU-II-633 from Lago Puyehue suggest Chaitén volcano to be its most likely origin. In that case, the inferred age for PU-II-633 from the core's age model, would suggest this unit could also correspond to ChaA1 (Fig. 6). Moreno et al. (2015a) suggest one, or more, of the bottom tephras in the Lago Teo sediment core correspond to Cha1, although the data are inconclusive. Given its northward dispersal, and its presence in the sediments of Lago Villarrica and Laguna Las Ranas, 400 km from source, it is highly likely that Cha1 is also present in the sediments of Lago Puyehue (Bertrand et al., 2008b). So far, Cha1 is the only marker that allows clear integration of Lake District records with those of the Southern SVZ (Osorno volcano and further south).

The tephrochronological framework for the Hualaihue region developed by Watt et al. (2011, Fig. 1) has identified a vast number of tephra deposits of moderately wide dispersal, especially from Calbuco volcano. From Fig. 6 it is however clear that none of these can currently be firmly correlated with other records due to a lack of chemical data in these records (e.g., Iglesias et al., 2012; Massaferro and Corley, 1998; Román-Ross et al., 2002; Tatur et al., 2002). Daga et al. (2008, 2010) have inferred several tephras in short cores from the Lago Nahuel Huapi area to originate from Calbuco volcano, so it is most likely that some of the Calbuco deposits described and well-dated by Watt et al. (2011) have left useful markers in the long sedimentary archives from the same area as well.

Further south of Chaitén, Hudson (45.91°S, 72.95°W) is one of the more important fairly regular producers of widespread marker horizons throughout the postglacial. Several units, especially Ho, H1 and H2 have been recognised in multiple records (e.g., Carel et al., 2011; Haberle and Lumley, 1998; Naranjo and Stern, 1998; Prieto et al., 2013; Stern, 2008; Stern et al., 2015; 2016; Van Daele et al., 2016; Weller et al., 2014), although there is still a lot of uncertainty on the age of H1 in particular. A "best average" of 7750 ± 95 (1σ) cal a BP was suggested by Prieto et al. (2013) based on a selection of 13 radiocarbon dates. Bayesian modelling, following the procedures outlined in Section 3.1, of new AMS ages presented by Stern et al. (2016) suggests an age of 7.90 ± 0.02 cal ka BP for terrestrial sections, but 8.52 ± 0.08 cal ka BP for lacustrine sections. Correlations of Hudson deposits based on geochemical data are especially complicated by the fact that Hudson shows a wide range of compositions within most of its tephra deposits, spanning from basaltic andesite to rhyolite. There is thus still plenty of scope to improve the existing tephrochronological framework of Hudson volcano, and integrate proximal with medial – distal records.

4.4. Temporal trends in volcanic activity

Our regional age model constructed from the integration of terrestrial and lacustrine sedimentary archives between 38.5 and 41°S provides a view of the large-scale volcanic activity that has impacted the Chilean Lake District, especially in the northern part, throughout the postglacial period. Although a number of moderate-scale (magnitude 3) eruptions are also included in the model, because their deposits are useful markers to synchronise different sections (e.g., HUA1, Quet3; Table 1, Fig. 3), our age model

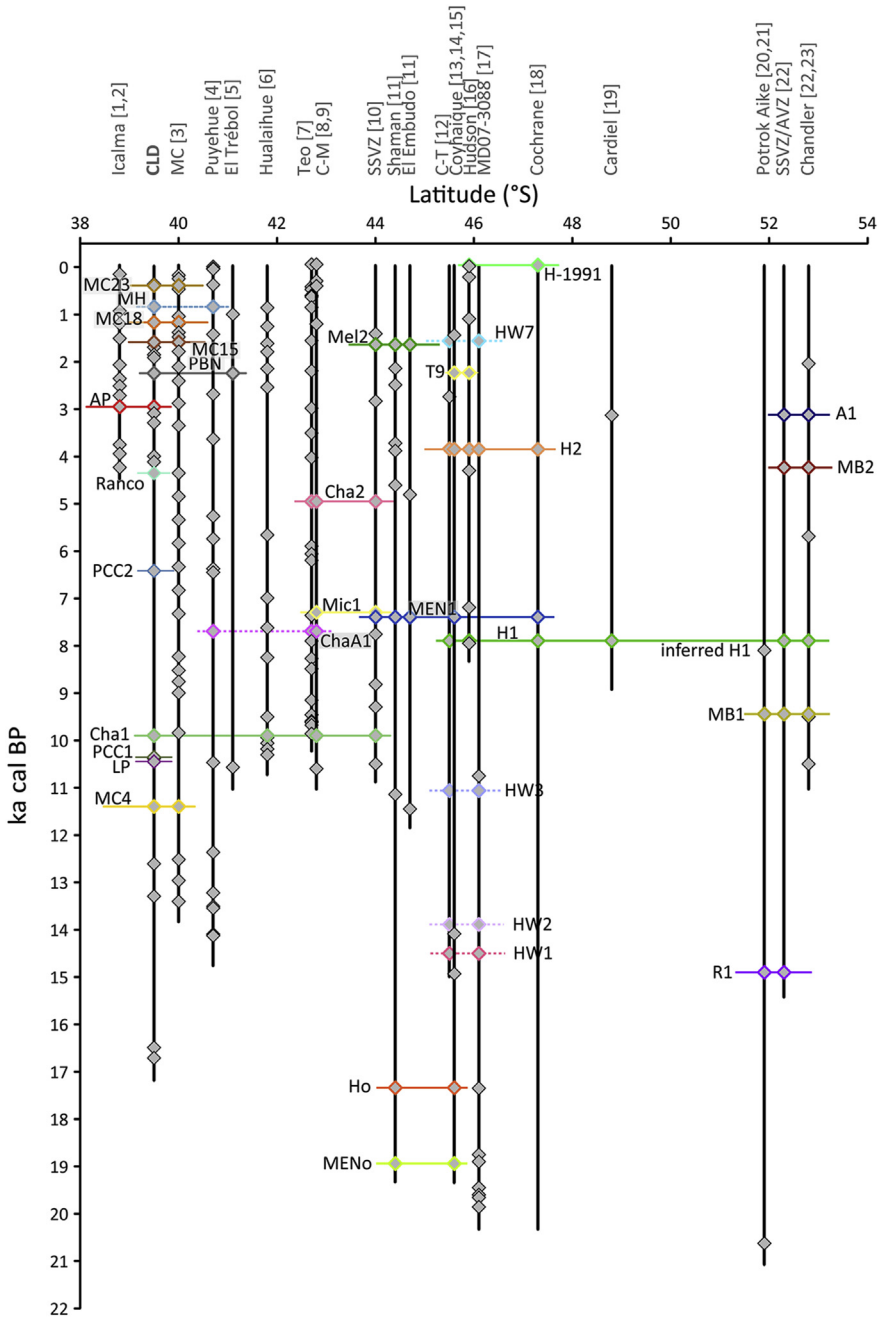

Fig. 6. Schematic illustration of the potential, and limitations, of synchronising sedimentary archives using widespread tephra deposits in southern Chile and Argentina (~39–53°S). Logs represent individual lake sediment cores or compiled stratigraphic sequences from terrestrial exposures. Tephra deposits are indicated by diamonds: those uncorrelated between different sections are indicated in grey, others in colour. The correlated and dated tephras, highlighted by horizontal bars, are all scaled to the same timeframe: assigned ages are either modelled using Bayesian analysis (Watt et al., 2013a; this work) or calibrated ages from published literature. Only studies presenting chemical data on tephra deposits are taken up in this graph. Tephras without assigned ages are not shown so some records in fact contain many more tephras than indicated on the figure. Dashed lines indicate suggested correlations which should be verified with additional chemical data. Tephra names taken from literature; MH: Mil Hojas; PBN: Playas Blancas Negras; AP: Alpehue Pumice; LP: Llaima Pumice. Ages for non-correlated tephras are taken from literature, and usually based on interpolations of radiocarbon dates on lake sediments. Ages for the Lago Puyehue core (Bertrand et al., 2008b) have been re-estimated using a set of 6 additional radiocarbon dates (Bertrand et al., unpublished data) and the pre-aged soil carbon effect correction method described by Bertrand et al. (2012). A number of key units within the Lake District are expected to be widespread and have a strong potential as chronological markers (Ranco, PCC2, PCC1 and Llaima Pumice). For completeness, and to illustrate the potential of regional-scale tephrochronology in southern Chile and Argentina, sections south of Chaitén are shown as well, with especially Hudson volcano acting as a regular source of regional-scale marker horizons (labelled H or HW, after respective literature sources). CLD: Chilean Lake District; MC: Mocho-Choshuenco; C–M: Chaitén-Michinmahuida; SSVZ: Southern Southern Volcanic Zone; C–T: Chonos-Taitao; AVZ: Austral Volcanic Zone. References: [1] Juvigné et al., 2008; [2] Bertrand et al., 2008a; [3] Rawson et al., 2015; [4] Bertrand et al., 2008b, only thickest tephras shown; [5] Villarosa et al., 2006; [6] Watt et al., 2011; [7] Moreno et al., 2015a; [8] Amigo et al., 2013; [9] Watt et al., 2013b; [10] Naranjo and Stern 2004; [11] Stern et al., 2015; [12] Haberle and Lumley 1998; [13] Weller et al., 2014; [14] Weller et al., 2015; [15] Van Daele et al., 2016; [16] Naranjo and Stern 1998; [17] Carel et al., 2011; [18] Stern et al., 2016; [19] Markgraf et al., 2003; [20] Haberzettl et al., 2009; [21] Wastegård et al., 2013; [22] Stern 2008; [23] Kilian et al., 2003. (For interpretation of the references to colour in this figure legend, the reader is referred to the web version of this article.)

provides a more complete view of the temporal variability of large-scale (magnitude 4 and larger) explosive volcanic eruptions in the region than was previously possible (Watt et al., 2013a).

Onset of the last deglaciation in the Lake District is thought to have started at ~17.8 cal ka BP, with relatively fast glacial retreat and recovery to humid conditions and dense forest vegetation within ~1000 years (Moreno et al., 2015b). This is broadly consistent with the suggested synchronous onset of deglaciation in southern Chile at 17.50–17.15 cal ka BP, with a second warming step at 15.35–15.65 cal ka BP in the Lake District (McCulloch et al., 2000). The lakes in this area are mostly moraine-dammed and have started accumulating sediments during deglaciation as glacial tills, as well as during the deglaciation process (Charlet et al., 2008; Heirman et al., 2011). There are no pre- or syn-glacial tephra records available within the Chilean Lake District. This would mean that the two earliest marker beds in our record result from eruptions that occurred very soon after the first warming step (Licán Ignimbrite, 16.71 ± 0.17 cal ka BP, and Quet1, 16.49 ± 0.31 cal ka BP; Table 1, Fig. 5). Between ca. 13.0 and 9.5 ka, our age model suggests that a period of relatively intense volcanic activity affected the Lake District, with four magnitude 5–6 events from four different volcanoes (Mocho-Choshuenco, Llaima, Puyehue-Cordón Caulle and Chaitén). This pulse is followed by a relatively quiet period between 9.5 and 4.5 ka, during which only one significant event is recorded in our tephrochronological model (PCC2, 6.42 ± 0.16 cal ka BP; Table 1, Fig. 5). The lacustrine records show that volcanic activity was still ongoing during this period, but that it was largely restricted to small or moderate-scale eruptions of relatively mafic composition, e.g., from Villarrica volcano. Following the Ranco Pumice eruption, a phase of renewed larger-scale activity starts with up to eight magnitude 4–5 events from five different volcanoes (Puyehue-Cordón Caulle, Villarrica, Sollipulli, Antillanca and Mocho-Choshuenco). A similar tripartite pattern of activity is observed in the detailed post-glacial stratigraphic eruption records of Mocho-Choshuenco volcano (Rawson et al., 2016).

The lacustrine records studied here do not all span the entire postglacial period. The LR0901B core of Laguna Las Ranas (Table 2) however does have glacial clay at its base, deposited immediately after ice retreat, and the VILLAR1 core from Lago Villarrica (Wiemer et al., 2015, Table 2) contains the early postglacial MC4 deposit (Table 1). From the integration with terrestrial records, which show tephra deposits occurring on top of the glacially eroded crystalline basement rocks, either immediately or separated by a thin soil horizon, we are confident that we have captured the entire postglacial history of large-magnitude explosive volcanic activity impacting the region. Onset of deglaciation is thought to have been associated with relatively fast expansion of dense forest vegetation, and followed again by a short return to cold and wetter conditions in the Lake District (e.g., Bertrand et al., 2008a; Moreno et al., 2015b). Climatic conditions during the earliest postglacial period may not have been optimal for the preservation of deposits, which could explain why our record only shows two events in this early period, with a gap until some of the largest recorded eruptions. The early-to-mid-Holocene period in our study area was characterised by a warm and dry climate and the development of more grassy vegetation at the expense of forest (Abarzúa et al., 2004; Bertrand et al., 2008a; Lamy et al., 2010; Moreno and León, 2003; Vargas-Ramirez et al., 2008). These Holocene climatic variations may have had an adverse impact on the preservation of small-to-moderate-scale deposits, especially on land. However, despite limited river transport into the lakes in these dry periods, we would still expect to see some evidence, if large eruptions had impacted the area, including by direct fallout over the lake surface for at least some events. We therefore suggest that there is indeed an early-to-mid-Holocene period in the Chilean Lake District of relative quiescence of volcanic activity, in terms of magnitude of eruptions. Eruptions still frequently occurred in the area; however no large events are detected.

The relatively quiet period is followed again by resurgence in activity, with larger eruptions occurring again, typically of dacitic to rhyolitic composition. This temporal variability in large-scale volcanic activity may be controlled by external processes like deglaciation, and attendant changes in erosion rate, influencing the loading on the crust (e.g., Jellinek et al., 2004; Nowell et al., 2006; Watt et al., 2013a); and thereby influencing the stress distribution around crustal magma reservoirs, as suggested for Mocho-Choshuenco (Rawson et al., 2016). To further evaluate the temporal behaviour of volcanic activity in this segment of the continental arc however, the record needs to be supplemented with data on smaller-scale eruptions to constrain overall eruptive rates, which also need to be evaluated for each volcano individually (e.g., Rawson et al., 2015, 2016). Given that the lacustrine records show evidence of continued, but small-scale, activity during the early-to-mid-Holocene, it is clear that the overall eruptive *frequency* may not have varied significantly through time, but the eruptive *rate* (typically expressed in km^3/ky, e.g., Rawson et al., 2016) has.

5. Summary

The tephrochronological framework for the Chilean Lake District developed here holds great promise to synchronise various palaeoenvironmental, palaeoclimatological and palaeoseismological records in the area and beyond. We integrated terrestrial and lacustrine tephrostratigraphic records in the area between 38 and 42°S and developed a composite chronological model using geochemical data (glass major element compositions) and Bayesian modelling on radiocarbon dates acquired on proximal deposits. This results in the definition of 25 well-characterised and precisely dated tephra marker horizons, from large explosive eruptions which can be used to integrate various records and extend the tephrochronological framework further south. Some of the key marker horizons that were previously known from the literature now have well-defined chemical compositions and improved age estimates. This includes the andesitic-dacitic Llaima Pumice from Llaima volcano (10.45 ± 0.13 cal ka BP) and the rhyodacitic Mil Hojas from Puyehue-Cordón Caulle (0.84 ± 0.18 cal ka BP). The early-Holocene Cha1 deposit from Chaiten volcano (9.90 ± 0.25 cal ka BP) is recognised 400 km from source and preserved as a visible ash layer incorporated within the sediments of Lago Villarrica and Laguna Las Ranas and is one of the most important regional marker horizons in the area, together with MC4 (Neltume Pumice) from Mocho-Choshuenco (11.40 ± 0.81 cal ka BP). A number of previously poorly described or undescribed units are defined for Quetrupillan and Puyehue-Cordón Caulle volcanoes, including Puesco Pumice (1.92 ± 0.07 cal ka BP) and Ranco Pumice (4.35 ± 0.33 cal ka BP). Tephra deposit thickness in lacustrine records does not seem to be a reliable measure for primary depositional thickness, as a result of tephra transport by rivers into the lakes, especially those with large catchments. However, because of this sensitivity to tephra input by river transport, such lakes do potentially provide the most complete tephrostratigraphic records in terms of recording discrete events. In the Chilean Lake District, regional markers from large explosive eruptions impacting the region are temporally concentrated in the early postglacial, between ca. 13.0 and 9.5 ka, and in the late-Holocene, since ca. 4.5 ka. Between that, a period of relative quiescence seems to exist during which almost no deposits of regional-scale explosive eruptions are detected, providing insights into temporal variability of volcanic activity in the region and the possible control of deglaciation on the occurrence of large-magnitude eruptions.

Acknowledgements

KF and HR are supported by the Natural Environment Research Council (NERC) grant NE/I013210/1. MVD is supported by Research Foundation (FWO) – Flanders. JM acknowledges support of Chilean FONDECYT project 1150346, FWO-Flanders and the Swiss National Science Foundation (grant 133481). Sediment cores were acquired with funding from FWO-Flanders, the Special Research Fund (BOF) of Ghent University, and the Belgian Science Policy (BELSPO). DMP and TAM are supported by and contribute to the NERC National Centre for Earth Observation, which includes the Centre for the Observation and Modelling of Earthquakes, Volcanoes and Tectonics (COMET+). We are grateful to CONAF (Chile) and APN (Argentina) for providing us permission to work in national parks. Radiocarbon dating was supported by the NERC Radiocarbon Facility NRCF010001 (allocation number 1813.0414). We thank Norman Charnley, Victoria Smith, Jamie Long, Steve Moreton, Alejandro Baeza Gonzalez, Pia Leiva Cardenas, Daniela Rodriguez, Anthony Neyt, Sebastian Watt, Stephen Turner and Irina Papadimitriou for assistance during various stages of fieldwork, sample preparation and/or data acquisition. Acquisition of some PCC2011 data was funded by FWO-Flanders, grant 1.5.244.13N to SB. Editorial handling by Neil Roberts, and reviews by Charles Stern and two anonymous reviewers have helped improving this manuscript.

Appendix A. Supplementary data

Supplementary data related to this article can be found at http://dx.doi.org/10.1016/j.quascirev.2016.02.015.

References

Abarzúa, A.M., Villagrán, C., Moreno, P.I., 2004. Deglacial and postglacial climate history in east-central Isla Grande de Chiloé, southern Chile (43°S). Quat. Res. 62, 49–59.

Amigo, Á., Lara, L.E., Smith, V.C., 2013. Holocene record of large explosive eruptions from Chaitén and Michinmahuida Volcanoes, Chile. Andean Geol. 40, 227–248.

Bertrand, S., Araneda, A., Vargas, P., Jana, P., Fagel, N., Urrutia, R., 2012. Using the N/C ratio to correct bulk radiocarbon ages from lake sediments: insights from Chilean Patagonia. Quat. Geochronol. 12, 23–29.

Bertrand, S., Castiaux, J., Juvigné, E., 2008b. Tephrostratigraphy of the late glacial and Holocene sediments of Puyehue Lake (southern volcanic zone, Chile, 40°S). Quat. Res. 70, 343–357.

Bertrand, S., Charlet, F., Charlier, B., Renson, V., Fagel, N., 2008a. Climate variability of southern Chile since the last glacial maximum: a continuous sedimentological record from Lago Puyehue (40°S). J. Paleolimnol. 39, 179–195.

Bertrand, S., Daga, R., Bedert, R., Fontijn, K., 2014. Deposition of the 2011–2012 Cordón Caulle tephra (Chile, 40°S) in lake sediments: implications for tephrochronology and volcanology. J. Geophys. Res. Earth Surf. 119, 2555–2573.

Blockley, S.P.E., Bronk Ramsey, C., Pyle, D.M., 2008. Improved age modelling and high-precision age estimates of late Quaternary tephras, for accurate palaeoclimate reconstruction. J. Volcanol. Geotherm. Res. 177, 251–262.

Blockley, S.P.E., Lane, C.S., Hardiman, M., Rasmussen, S.O., Seierstad, I.K., Steffensen, J.P., Svensson, A., Lotter, A.F., Turney, C.S.M., Bronk Ramsey, C., 2012. Synchronisation of palaeoenvironmental records over the last 60,000 years, and an extended INTIMATE1 event stratigraphy to 48,000 b2k. Quat. Sci. Rev. 36, 2–10.

Boës, X., Fagel, N., 2008. Relationships between southern Chilean varved lake sediments, precipitation and ENSO for the last 600 years. J. Paleolimnol. 39, 237–252.

Bonadonna, C., Biass, S., Costa, A., 2015. Physical characterization of explosive volcanic eruptions based on tephra deposits: propagation of uncertainties and sensitivity analysis. J. Volcanol. Geotherm. Res. 296, 80–100.

Bronk Ramsey, C., 2009. Bayesian analysis of radiocarbon dates. Radiocarbon 51, 337–360.

Carel, M., Siani, G., Delpech, G., 2011. Tephrostratigraphy of a deep-sea sediment sequence off the south Chilean margin: new insight into the Hudson volcanic activity since the last glacial period. J. Volcanol. Geotherm. Res. 208, 99–111.

Charlet, F., De Batist, M., Chapron, E., Bertrand, S., Pino, M., Urrutia, R., 2008. Seismic stratigraphy of Lago Puyehue (Chilean Lake District): new views on its deglacial and Holocene evolution. J. Paleolimnol. 39, 163–177.

Costantini, L., Pioli, L., Bonadonna, C., Clavero, J., Longchamp, C., 2011. A Late Holocene explosive mafic eruption of Villarrica volcano, southern Andes: the Chaimilla deposit. J. Volcanol. Geotherm. Res. 200, 143–158.

Daga, R., Ribeiro Guevara, S., Sánchez, M.L., Arribére, M., 2008. Source identification of volcanic ashes by geochemical analysis of well preserved lacustrine tephras in Nahuel Huapi National Park. Appl. Radiat. Isot. 66, 1325–1336.

Daga, R., Ribeiro Guevara, S., Sánchez, M.L., Arribére, M., 2010. Tephrochronology of recent events in the Andean range (northern Patagonia): spatial distribution and provenance of lacustrine ash layers in the Nahuel Huapi National Park. J. Quat. Sci. 25, 1113–1123.

Daggitt, M., Mather, T., Pyle, D., Page, S., 2014. AshCalc-a new tool for the comparison of the exponential, power-law and Weibull models of tephra deposition. J. Appl. Volcanol. 3, 7.

Davies, S.M., Abbott, P.M., Pearce, N.J.G., Wastegård, S., Blockley, S.P.E., 2012. Integrating the INTIMATE records using tephrochronology: rising to the challenge. Quat. Sci. Rev. 36, 11–27.

Eggert, S., Walter, T.R., 2009. Volcanic activity before and after large tectonic earthquakes: observations and statistical significance. Tectonophysics 471, 14–26.

Fletcher, M.-S., Moreno, P.I., 2012. Vegetation, climate and fire regime changes in the Andean region of southern Chile (38°S) covaried with centennial-scale climate anomalies in the tropical Pacific over the last 1500 years. Quat. Sci. Rev. 46, 46–56.

Fontijn, K., Costa, F., Sutawidjaja, I., Newhall, C.G., Herrin, J.S., 2015. A 5000-year record of multiple highly explosive mafic eruptions from Gunung Agung (Bali, Indonesia): implications for eruption frequency and volcanic hazards. Bull. Volcanol. 77, 59.

Fontijn, K., Lachowycz, S.M., Rawson, H., Pyle, D.M., Mather, T.A., Naranjo, J.A., Moreno-Roa, H., 2014. Late Quaternary tephrostratigraphy of southern Chile and Argentina. Quat. Sci. Rev. 89, 70–84.

Haberle, S.G., Lumley, S.H., 1998. Age and origin of tephras recorded in postglacial lake sediments to the west of the southern Andes, 44°S to 47°S. J. Volcanol. Geotherm. Res. 84, 239–256.

Haberzettl, T., Anselmetti, F.S., Bowen, S.W., Fey, M., Mayr, C., Zolitschka, B., Ariztegui, D., Mauz, B., Ohlendorf, C., Kastner, S., Lücke, A., Schäbitz, F., Wille, M., 2009. Late Pleistocene dust deposition in the Patagonian steppe – extending and refining the paleoenvironmental and tephrochronological record from Laguna Potrok Aike back to 55 ka. Quat. Sci. Rev. 28, 2927–2939.

Heirman, K., De Batist, M., Charlet, F., Moernaut, J., Chapron, E., Brümmer, R., Pino, M., Urrutia, R., 2011. Detailed seismic stratigraphy of Lago Puyehue: implications for the mode and timing of glacier retreat in the Chilean lake district. J. Quat. Sci. 26, 665–674.

Henríquez, W.I., Moreno, P.I., Alloway, B.V., Villarosa, G., 2015. Vegetation and climate change, fire-regime shifts and volcanic disturbance in Chiloé continental (43°S) during the last 10,000 years. Quat. Sci. Rev. 123, 158–167.

Heusser, C.J., Heusser, L.E., Lowell, T.V., 1999. Paleoecology of the southern Chilean lake district-Isla Grande de Chiloé during Middle–late Llanquihue Glaciation and Deglaciation. Geogr. Ann. Ser. A Phys. Geogr. 81, 231–284.

Heusser, C.J., Rabassa, J., Brandani, A., Stuckenrath, R., 1988. Late-Holocene vegetation of the Andean Araucaria region, Province of Neuquén, Argentina. Mt. Res. Dev. 8, 53–63.

Hoganson, J.W., Ashworth, A.C., 1992. Fossil beetle evidence for climatic change 18,000–10,000 years B.P. in south-central Chile. Quat. Res. 37, 101–116.

Hogg, A.G., Hua, Q., Blackwell, P.G., Niu, M., Buck, C.E., Guilderson, T.P., Heaton, T.J., Palmer, J.G., Reimer, P.J., Reimer, R.W., Turney, C.S.M., Zimmerman, S.R.H., 2013. SHCal13 southern hemisphere calibration, 0-50,000 years cal BP. Radiocarbon 55, 1889–1903.

Howarth, J.D., Fitzsimons, S.J., Jacobsen, G.E., Vandergoes, M.J., Norris, R.J., 2013. Identifying a reliable target fraction for radiocarbon dating sedimentary records from lakes. Quat. Geochronol. 17, 68–80.

Huybers, P., Langmuir, C., 2009. Feedback between deglaciation, volcanism, and atmospheric CO2. Earth Planet. Sci. Lett. 286, 479–491.

Iglesias, V., Whitlock, C., Bianchi, M.M., Villarosa, G., Outes, V., 2012. Climate and local controls of long-term vegetation dynamics in northern Patagonia (Lat 41°S). Quat. Res. 78, 502–512.

Jara, I.A., Moreno, P.I., 2014. Climatic and disturbance influences on the temperate rainforests of northwestern Patagonia (40°S) since ~14,500 cal yr BP. Quat. Sci. Rev. 90, 217–228.

Jellinek, A.M., Manga, M., Saar, M.O., 2004. Did melting glaciers cause volcanic eruptions in eastern California? J. Geophys. Res. 109, B09206.

Jochum, K.P., Stoll, B., Herwig, K., Willbold, M., Hofmann, A.W., Amini, M., Aarburg, S., Abouchami, W., Hellebrand, E., Mocek, B., Raczek, I., Stracke, A., Alard, O., Bouman, C., Becker, S., Dücking, M., Brätz, H., Klemd, R., de Bruin, D., Canil, D., Cornell, D., de Hoog, C.-J., Dalpé, C., Danyushevsky, L., Eisenhauer, A., Gao, Y., Snow, J.E., Groschopf, N., Günther, D., Latkoczy, C., Guillong, M., Hauri, E.H., Höfer, H.E., Lahaye, Y., Horz, K., Jacob, D.E., Kasemann, S.A., Kent, A.J.R., Ludwig, T., Zack, T., Mason, P.R.D., Meixner, A., Rosner, M., Misawa, K., Nash, B.P., Pfänder, J., Premo, W.R., Sun, W.D., Tiepolo, M., Vannucci, R., Vennemann, T., Wayne, D., Woodhead, J.D., 2006. MPI-DING reference glasses for in situ microanalysis: new reference values for element concentrations and isotope ratios. Geochem. Geophys. Geosyst. 7, Q02008.

Juvigné, E., Bertrand, S., Heuschen, B., Tallier, E., 2008. Tephrostratigraphy of lake sediments located in an active geodynamic setting: lessons from Lake Icalma (Chile, southern volcanic zone, 38°S). Quaternaire 19, 175–189.

Kilian, R., Hohner, M., Biester, H., Wallrabe-Adams, H.J., Stern, C.R., 2003. Holocene peat and lake sediment tephra record from the southernmost Chilean Andes (53-55°S). Rev. Geol. Chile 30, 23–37.

Kuehn, S.C., Froese, D.G., Shane, P.A.R., INTAV Intercomparison Participants, 2011. The INTAV intercomparison of electron-beam microanalysis of glass by

tephrochronology laboratories: results and recommendations. Quat. Int. 246, 19–47.
Lamy, F., Kilian, R., Arz, H.W., François, J.-P., Kaiser, J., Prange, M., Steinke, T., 2010. Holocene changes in the position and intensity of the southern westerly wind belt. Nat. Geosci. 3, 695–699.
Lara, L.E., Moreno, H., Naranjo, J.A., Matthews, S., Pérez de Arce, C., 2006. Magmatic evolution of the Puyehue - Cordón Caulle volcanic complex (40° S), southern Andean volcanic zone: from shield to unusual rhyolitic fissure volcanism. J. Volcanol. Geotherm. Res. 157, 343–366.
Lemarchand, N., Grasso, J.-R., 2007. Interactions between earthquakes and volcano activity. Geophys. Res. Lett. 34, L24303.
Lohmar, S., Parada, M., Gutiérrez, F., Robin, C., Gerbe, M.C., 2012. Mineralogical and numerical approaches to establish the pre-eruptive conditions of the mafic Licán Ignimbrite, Villarrica volcano (Chilean southern Andes). J. Volcanol. Geotherm. Res. 235–236, 55–69.
Lohmar, S., Robin, C., Gourgaud, A., Clavero, J., Parada, M., Moreno, H., Ersoy, O., López-Escobar, L., Naranjo, J., 2007. Evidence of magma-water interaction during the 13,800 years BP explosive cycle of the Licán Ignimbrite, Villarrica volcano (southern Chile). Rev. Geol. Chile 34, 233–247.
Lowe, D.J., 2011. Tephrochronology and its application: a review. Quat. Geochronol. 6, 107–153.
Maclennan, J., Jull, M., McKenzie, D., Slater, L., Grönvold, K., 2002. The link between volcanism and deglaciation in Iceland. Geochem. Geophys. Geosyst. 3, 1062.
Markgraf, V., Bradbury, J.P., Schwalb, A., Burns, S.J., Stern, C., Ariztegui, D., Gilli, A., Anselmetti, F.S., Stine, S., Maidana, N., 2003. Holocene palaeoclimates of southern Patagonia: limnological and environmental history of Lago Cardiel, Argentina. Holocene 13, 581–591.
Massaferro, J., Corley, J., 1998. Environmental disturbance and chironomid palaeodiversity: 15 kyr BP of history at Lake Mascardi, Patagonia, Argentina. Aquat. Conserv. Mar. Freshw. Ecosyst. 8, 315–323.
McCulloch, R.D., Bentley, M.J., Purves, R.S., Hulton, N.R.J., Sugden, D.E., Clapperton, C.M., 2000. Climatic inferences from glacial and palaeoecological evidence at the last glacial termination, southern South America. J. Quat. Sci. 15, 409–417.
Moernaut, J., De Batist, M., Charlet, F., Heirman, K., Chapron, E., Pino, M., Brümmer, R., Urrutia, R., 2007. Giant earthquakes in south-central Chile revealed by Holocene mass-wasting events in Lake Puyehue. Sediment. Geol. 195, 239–256.
Moernaut, J., Van Daele, M., Heirman, K., Fontijn, K., Strasser, M., Pino, M., Urrutia, R., De Batist, M., 2014. Lacustrine turbidites as a tool for quantitative earthquake reconstruction: new evidence for a variable rupture mode in south-central Chile. J. Geophys. Res. Solid Earth 119, 1607–1633.
Moernaut, J., Van Daele, M., Strasser, M., Clare, M., Heirman, K., Viel, M., Cardenas, J., Kilian, R., Ladrón de Guevara, B., Pino, M., Urrutia, R., De Batist, M., 2016. Lacustrine turbidites produced by surficial slope sediment remobilization: a mechanism for continuous and sensitive turbidite paleoseismic records. Mar. Geol. http://dx.doi.org/10.1016/j.margeo.2015.10.009 (in press).
Moreno, H., Clavero, J.R., 2006. Geología del Volcán Villarrica, Regiones de la Araucanía y de Los Lagos. Carta Geol. Chile Ser. Geol. Básica 98. SERNAGEOMIN, Santiago.
Moreno, P.I., 1997. Vegetation and climate near Lago Llanquihue in the Chilean lake district between 20200 and 9500 14C yr BP. J. Quat. Sci. 12, 485–500.
Moreno, P.I., Alloway, B.V., Villarosa, G., Outes, V., Henríquez, W.I., De Pol-Holz, R., Pearce, N.J.G., 2015a. A past-millennium maximum in postglacial activity from Volcán Chaitén, southern Chile. Geology 43, 47–50.
Moreno, P.I., Denton, G.H., Moreno, H., Lowell, T.V., Putnam, A.E., Kaplan, M.R., 2015b. Radiocarbon chronology of the last glacial maximum and its termination in northwestern Patagonia. Quat. Sci. Rev. 122, 233–249.
Moreno, P.I., Jacobson, G.L., Lowell, T.V., Denton, G.H., 2001. Interhemispheric climate links revealed by a late-glacial cooling episode in southern Chile. Nature 409, 804–808.
Moreno, P.I., León, A.L., 2003. Abrupt vegetation changes during the last glacial to Holocene transition in mid-latitude South America. J. Quat. Sci. 18, 787–800.
Naranjo, J.A., Moreno, H., 1991. Postglacial explosive activity at Llaima volcano, southern Andes (38° 45′S). Rev. Geol. Chile 18, 69–80.
Naranjo, J.A., Moreno, H., 2005. Geología del Volcán Llaima, Región de la Araucanía. In: Carta Geol. Chile Serie Geología Básica. No. 88. SERNAGEOMIN, Santiago.
Naranjo, J.A., Moreno, H., Emparan, C., Murphy, M., 1993. Recent explosive volcanism in the Sollipulli caldera, southern Andes (39°S). Rev. Geol. Chile 20, 167–191.
Naranjo, J.A., Stern, C.R., 1998. Holocene explosive activity of Hudson volcano, southern Andes. Bull. Volcanol. 59, 291–306.
Naranjo, J.A., Stern, C.R., 2004. Holocene tephrochronology of the southernmost part (42°30′ - 45°S) of Andean southern volcanic zone. Rev. Geol. Chile 31, 225–240.
Newhall, C.G., Self, S., 1982. The volcanic explosivity index (VEI) - an estimate of explosive magnitude for historical volcanism. J. Geophys. Res. 87, 1231–1238.
Nowell, D.A.G., Jones, M.C., Pyle, D.M., 2006. Episodic Quaternary volcanism in France and Germany. J. Quat. Sci. 21, 645–675.
Pavez, A., 1997. Geology and evolution history of the Quetrupillan volcanic complex, southern Andes, 39.5° S. In: VIII Geological Congres Chile – Actas 2, pp. 1443–1447.
Pearce, N.J.G., Abbott, P.M., Martin-Jones, C., 2014. Microbeam Methods for the Analysis of Glass in Fine-grained Tephra Deposits: a SMART Perspective on Current and Future Trends. Geol. Soc. London, Spec. Publ. 398, pp. 29–46.
Pistolesi, M., Cioni, R., Bonadonna, C., Elissondo, M., Baumann, V., Bertagnini, A., Chiari, L., Gonzales, R., Rosi, M., Francalanci, L., 2015. Complex dynamics of small-moderate volcanic events: the example of the 2011 rhyolitic Cordón Caulle eruption, Chile. Bull. Volcanol. 77, 3.
Ponomareva, V., Portnyagin, M., Davies, S., 2015. Tephra without borders: far-reaching clues into past explosive eruptions. Front. Earth Sci. 3, 83.
Prieto, A., Stern, C.R., Estévez, J.E., 2013. The peopling of the Fuego-Patagonian fjords by littoral hunter–gatherers after the mid-Holocene H1 eruption of Hudson volcano. Quat. Int. 317, 3–13.
Pyle, D.M., 1989. The thickness, volume and grainsize of tephra fall deposits. Bull. Volcanol. 51, 1–15.
Pyle, D.M., 1995. Assessment of the minimum volume of tephra fall deposits. J. Volcanol. Geotherm. Res. 69, 379–382.
Pyle, D.M., 2000. Sizes of volcanic eruptions. In: Sigurdsson, H., Houghton, B., Rymer, H., Stix, J., McNutt, S.R. (Eds.), Encyclopedia of Volcanoes. Academic Press, pp. 263–269.
Rawson, H., Naranjo, J.-A., Smith, V., Fontijn, K., Pyle, D.M., Mather, T.A., Moreno, H., 2015. The frequency and magnitude of post-glacial explosive eruptions at Volcán Mocho-Choshuenco, southern Chile. J. Volcanol. Geotherm. Res. 299, 103–129.
Rawson, H., Pyle, D.M., Mather, T.A., Smith, V.C., Fontijn, K., Lachowycz, S.M., Naranjo, J.A., 2016. The magmatic and eruptive response of arc volcanoes to deglaciation: insights from southern Chile. Geology. http://dx.doi.org/10.1130/G37504.1.
Román-Ross, G., Depetris, P.J., Arribére, M.A., Ribeiro Guevara, S., Cuello, G.J., 2002. Geochemical variability since the Late Pleistocene in Lake Mascardi sediments, northern Patagonia, Argentina. J. South Am. Earth Sci. 15, 657–667.
Schindlbeck, J.C., Freundt, A., Kutterolf, S., 2014. Major changes in the post-glacial evolution of magmatic compositions and pre-eruptive conditions of Llaima Volcano, Andean southern volcanic zone, Chile. Bull. Volcanol. 76, 1–22.
Siebert, L., Simkin, T., Kimberly, P., 2010. Volcanoes of the World, third ed. University of California Press, Berkeley.
Silva Parejas, C., Druitt, T.H., Robin, C., Moreno, H., Naranjo, J.A., 2010. The Holocene Pucón eruption of Volcan Villarrica, Chile: deposit architecture and eruption chronology. Bull. Volcanol. 72, 677–692.
Singer, B.S., Jicha, B.R., Harper, M.A., Naranjo, J.A., Lara, L.E., Moreno-Roa, H., 2008. Eruptive history, geochronology, and magmatic evolution of the Puyehue-Cordón Caulle volcanic complex, Chile. Geol. Soc. Am. Bull. 120, 599–618.
Sterken, M., Verleyen, E., Sabbe, K., Terryn, G., Charlet, F., Bertrand, S., Boës, X., Fagel, N., De Batist, M., Vyverman, W., 2008. Late Quaternary climatic changes in southern Chile, as recorded in a diatom sequence of Lago Puyehue (40°40′ S). J. Paleolimnol. 39, 219–235.
Stern, C.R., 2008. Holocene tephrochronology record of large explosive eruptions in the southernmost *Patagonian Andes*. Bull. Volcanol. 70, 435–454.
Stern, C.R., de Porras, M.E., Maldonado, A., 2015. Tephrochronology of the upper Rio Cisnes valley (44 S), southern Chile. Andean Geol. 42, 173–189.
Stern, C.R., Moreno, P.I., Henríquez, W.I., Villa-Martínez, R., Sagredo, E., Aravena, J.C., De Pol-Holz, R., 2016. Holocene tephrochronology around Cochrane (~47°S), southern Chile. Andean Geol. 43, 1–19.
Tatur, A., del Valle, R., Bianchi, M.-M., Outes, V., Villarosa, G., Niegodzisz, J., Debaene, G., 2002. Late Pleistocene palaeolakes in the Andean and Extra-Andean Patagonia at mid-latitudes of South America. Quat. Int. 89, 135–150.
Van Daele, M., Bertrand, S., Meyer, I., Moernaut, J., Vandoorne, W., Siani, G., Tanghe, N., Ghazoui, Z., Pino, M., Urrutia, R., De Batist, M., 2016. Late Quaternary evolution of Lago Castor (Chile, 45.6°S): timing of the deglaciation in northern Patagonia and evolution of the southern westerlies during the last 17 kyr. Quat. Sci. Rev. 133, 130–146.
Van Daele, M., Moernaut, J., Doom, L., Boes, E., Fontijn, K., Heirman, K., Vandoorne, W., Hebbeln, D., Pino, M., Urrutia, R., Brümmer, R., De Batist, M., 2015. A comparison of the sedimentary records of the 1960 and 2010 great Chilean earthquakes in 17 lakes: implications for quantitative lacustrine paleoseismology. Sedimentology 62, 1466–1496.
Van Daele, M., Moernaut, J., Silversmit, G., Schmidt, S., Fontijn, K., Heirman, K., Vandoorne, W., De Clercq, M., Van Acker, J., Wolff, C., Pino, M., Urrutia, R., Roberts, S.J., Vincze, L., De Batist, M., 2014. The 600 yr eruptive history of Villarrica volcano (Chile) revealed by annually laminated lake sediments. Geol. Soc. Am. Bull. 126, 481–498.
Vargas-Ramirez, L., Roche, E., Gerrienne, P., Hooghiemstra, H., 2008. A pollen-based record of late glacial–Holocene climatic variability in the southern lake district, Chile. J. Paleolimnol. 39, 197–217.
Villarosa, G., Outes, V., Hajduk, A., Crivelli Montero, E., Sellés, D., Fernández, M., Crivelli, E., 2006. Explosive volcanism during the Holocene in the upper Limay river Basin: the effects of ashfalls on human societies, northern Patagonia, Argentina. Quat. Int. 158, 44–57.
Wastegård, S., Veres, D., Kliem, P., Hahn, A., Ohlendorf, C., Zolitschka, B., 2013. Towards a late Quaternary tephrochronological framework for the southernmost part of South America – the Laguna Potrok Aike tephra record. Quat. Sci. Rev. 71, 81–90.
Watt, S.F.L., Gilbert, J.S., Folch, A., Phillips, J.C., Cai, X.M., 2015. An example of enhanced tephra deposition driven by topographically induced atmospheric turbulence. Bull. Volcanol. 77, 1–14.
Watt, S.F.L., Pyle, D.M., Mather, T.A., 2009. The influence of great earthquakes on volcanic eruption rate along the Chilean subduction zone. Earth Planet. Sci. Lett. 277, 399–407.
Watt, S.F.L., Pyle, D.M., Mather, T.A., 2013a. The volcanic response to deglaciation:

evidence from glaciated arcs and a reassessment of global eruption records. Earth Sci. Rev. 122, 77–102.
Watt, S.F.L., Pyle, D.M., Mather, T.A., 2013b. Evidence of mid- to late-Holocene explosive rhyolitic eruptions from Chaitén volcano, Chile. Andean Geol. 40, 216–226.
Watt, S.F.L., Pyle, D.M., Naranjo, J., Rosqvist, G., Mella, M., Mather, T.A., Moreno, H., 2011. Holocene tephrochronology of the Hualaihue region (Andean southern volcanic zone, ~42° S), southern Chile. Quat. Int. 246, 324–343.
Weller, D., Miranda, C.G., Moreno, P.I., Villa-Martínez, R., Stern, C.R., 2014. The large late-glacial Ho eruption of the Hudson volcano, southern Chile. Bull. Volcanol. 76, 1–18.
Weller, D.J., Miranda, C.G., Moreno, P.I., Villa-Martínez, R., Stern, C.R., 2015. Tephrochronology of the southernmost Andean southern volcanic zone, Chile. Bull. Volcanol. 77, 1–24.
Wiemer, G., Moernaut, J., Stark, N., Kempf, P., De Batist, M., Pino, M., Urrutia, R., de Guevara, B., Strasser, M., Kopf, A., 2015. The role of sediment composition and behavior under dynamic loading conditions on slope failure initiation: a study of a subaqueous landslide in earthquake-prone south-central Chile. Int. J. Earth Sci. 104, 1439–1457.